NUREG/CR-3330
SAND83-1178
R4, RP
Printed August 1983

# Vulnerability of Nuclear Power Plant Structures to Large External Fires

David E. Bennett

Prepared by
Sandia National Laboratories
Albuquerque, New Mexico 87185 and Livermore, California 94550
for the United States Department of Energy
under Contract DE-AC04-76DP00789

Prepared for
U. S. NUCLEAR REGULATORY COMMISSION

Available from
GPO Sales Program
Division of Technical Information and Document Control
U.S. Nuclear Regulatory Commission
Washington, D.C. 20555

and

National Technical Information Service
Springfield, Virginia 22161

NUREG/CR-3330
SAND83-1178
R4, RP

# VULNERABILITY OF NUCLEAR POWER PLANT STRUCTURES TO LARGE EXTERNAL FIRES

David E. Bennett

Date Published: August 1983

Sandia National Laboratories
Albuquerque, New Mexico 87185
operated by
Sandia Corporation
for the
US Department of Energy

Prepared for
Division of Risk Analysis
Office of Nuclear Regulatory Research
US Nuclear Regulatory Commission
Washington, DC 20555
Under Memorandum of Understanding DOE 40-550-75
NRC FIN No. A1214

## ABSTRACT

This report examines the inherent vulnerability of nuclear power plant structures to the thermal environments arising from large, external fires. The inherent vulnerability is the capacity of the concrete safety-related structures to absorb thermal loads without exceeding the appropriate thermal and structural design criteria. The potential sources of these thermal environments are large, offsite fires arising from accidents involving the transportation or storage of large quantities of flammable gases or liquids.

A realistic thermal response analysis of a concrete panel was performed using three limiting criteria: temperature at the first rebar location, erosion and ablation of the front (exterior) surface due to high heat fluxes, and temperature at the back (interior) surface. The results of this analysis yield a relationship between incident heat flux and the maximum allowable exposure duration.

A simple fire analysis method was developed to predict the thermal flux incident upon a target as a function of range. A key feature is the use of an experimentally observed specific power emitted from the surface of large fires.

Example calculations for the break of a 0.91 m (3') diameter high-pressure natural gas pipeline and a 1 $m^2$ hole in a 2-1/2 million gallon gasoline tank show that the resulting fires do not pose a significant hazard for ranges of 500 m or greater.

TABLE OF CONTENTS

LIST OF FIGURES

# LIST OF TABLES

## ACKNOWLEDGMENT

The author would like to thank Douglas Cline for performing the CINDA calculations and for his many helpful suggestions and discussions, Gilbert Weigand for his help on the Appendix, and David Lee for reviewing this work.

# 1.0 INTRODUCTION

This report examines the inherent vulnerability of nuclear power plant structures to potential thermal environments arising from large, external fires. The inherent vulnerability is the capacity of the concrete safety-related structures to absorb thermal loads without exceeding the appropriate thermal and structural design criteria. The sources of these thermal environments are large, offsite fires arising from accidents involving the transportation or storage of large quantities of flammable gases or liquids.

## 1.1 Background

This work is part of a program to evaluate the hazards to nuclear power plants due to nearby, but offsite, accidents involving hazardous materials. Five generic hazardous environment categories were identified in a preliminary assessment:[1] toxic, anoxic, corrosive, overpressure, and thermal. This report is a follow-on to the work described in Reference 1.

In Reference 1, the hazards from thermal environments due to fires involving truck or rail car quantities of flammable fluids burning at an accident site assumed 500 m from the plant were determined to be negligible. Note that for about 90 percent of the nuclear power plants in the US, the distance from a safety-related structure to the exclusion area boundary is greater than 500 m. Thus, road and rail transport of flammable materials do not pose a thermal threat to the plant if the fire occurs at the offsite accident location.

There remained to be considered the cases of: (1) delayed ignition of a vapor cloud, which could occur in close proximity to plant structures, and (2) much larger fires involving pipeline or storage facilities. In the first case, the fire duration would be short, on the order of 10 seconds. But the heat flux (units of $kW/m^2$) incident upon a plant building could be essentially the same as that emitted from the surface of the fireball, due to small standoff distances. In the second case, there would still be a moderate standoff distance from the fire to the plant to offer some protection, but the fire could be much larger than for the rail car case and the fire duration could be on the order of 1 to 10 hours or longer.

A wide variety of flammable fluids are found in commerce in the United States. In terms of resultant fire characteristics, a few categories or types of fuels appear sufficient for vulnerability modeling:

1. LNG -- liquified natural gas (cryogenic liquid, ambient pressure)
2. NG -- natural gas (compressed gas, ambient temperature)
3. LPG -- liquified petroleum gas (liquid under pressure, ambient temperature)
4. Liquid Products -- gasoline, kerosene, etc. (volatile and semivolatile liquids, ambient temperature, and pressure)
5. Crude-Oil -- less volatile than liquid products.

The storage conditions listed in parentheses are for normal or nonaccident environments. This report will consider natural gas and liquid products as examples. Appropriate release and fire models are then used to estimate fire size and thermal output for a reasonable range of accident conditions.

## 1.2 Analysis Methodology

The evaluation of the hazard which large fires could pose to nuclear power plants can be subdivided into two relatively independent parts. The first is a thermal response analysis of concrete panels, which defines the capacity of concrete structures to absorb heat without exceeding the thermal (and structural) design criteria. The second part is an estimation of the thermal output of large fires. Combining these results defines a relationship between standoff distance and exposure time as a function of various parameters describing the fire.

The thermal response analysis uses a realistic conduction model for concrete wall panels typical of safety related structures at nuclear power plants. A wall thickness of 0.61 m (2 feet) was assumed. The effects of reradiation from the (hot) front surface, convective cooling of the back surface, and ablation or decomposition of the front surface due to high heat flux-high temperature reactions, are included. Three criteria were used in estimating the resulting thermal capacity: a limit for erosion of the front surface to one-half of the distance to the first rebar, a maximum temperature at the first rebar location, and a maximum temperature at the back (inside) surface of the wall. The results of this analysis can be expressed as a function of incident heat flux versus maximum allowable exposure time.

The fire analysis uses relatively simple and realistic (but still conservative) models for estimating the size of a large fire and the radiative component of the thermal output. The analysis considers the chemical and physical properties of the flammable fluid, the fuel combustion rate, combustion efficiency, air entrainment, shape factors, and standoff

distance. The objective of this analysis is to express the thermal flux incident upon a target (eg, the plant) as a function of range and as few other variables as is possible, such that the results are realistic bounds for actual severe thermal environments.

## 1.3 Design Criteria for Concrete Structures

The concrete structures at nuclear power plants are currently designed to meet a variety of loads and environments. Reactor containment buildings are designed to withstand the elevated temperatures due to loss-of-coolant accidents. This is accomplished by a combination of containment cooling systems to ensure that the concrete structure itself remains within acceptable temperature limits. The American Concrete Institute[2] and the American Society of Mechanical Engineers[3] have specified the following maximum temperatures for concrete:

| | Maximum Allowable Temperature | |
|---|---|---|
| | Bulk | Local |
| Short Term (ie, following accidents) | 177°C (350°F) | 343°C (650°F) |
| Long Term | 66°C (150°F) | 93°C (200°F) |

Considering the large scale of potential fires, a considerable portion of a building could be exposed for several hours. The outer surfaces of concrete wall panels will, under high heat fluxes, be heated to much higher temperatures than any of the above criteria would allow. The structurally significant portion of the wall (the interior region containing the reinforcing steel) must be maintained within the temperature limit. For this interior region, the extent of the exposure would suggest the use of the bulk criterion in the above table rather than the local one, while the relatively short exposure times expected would correspond to a short-term condition, as compared to long term. For this study, the short-term, bulk temperature criterion will be used to define an acceptable temperature limit at the first rebar location. This will ensure that the entire interior region remains within the limit.

Additionally, for heat fluxes above 350 to 400 $kW/m^2$, erosion or ablation can occur due to chemical decomposition of the concrete surface. A criterion for how much of the outer portion of the concrete wall can be sacrificed due to

high temperature, ablation, or erosion can be developed from seismic response considerations.

The flexing of a reinforced concrete panel under seismic loadings results in cracking of the outer layer of concrete (between the surface and the first layer of reinforcing steel). During each oscillation, the convex surface is in tension, and hence fine cracking occurs. In a seismic safety analysis, no credit for strength is given to this outer layer.[17] For the thermal response analysis in this work, a reasonable criterion would be to apply the short-term, bulk temperature criterion at the first rebar location and allow higher temperatures in the outer layer. For an erosion-ablation criterion, loss of one-half of the outer layer would not result in a reduction of seismic capacity (other than the loss of mass).

The final criterion involves setting a maximum allowable temperature for the inside of the concrete wall. Since this would apply to the auxiliary and control buildings, safety-related equipment mounted on the inside surface should not be compromised. A reasonable maximum allowable temperature is 50°C (120°F). As will be seen later, this criterion is never exceeded; rather, the thermal capacity is controlled by the allowable temperature rise at the first rebar location.

In summary, three thermal criteria are chosen to define acceptable levels of exposure from large-scale fires:

| Thermal Criteria | Description |
|---|---|
| 1 | Temperature at the first rebar location not to exceed 177°C (350°F). |
| 2 | Thermal decomposition (erosion) not to penetrate more than one-half the distance to the first rebar. |
| 3 | Temperature of the interior surface not to exceed 50°C (120°F). |

## 2.0 THERMAL RESPONSE ANALYSIS OF A CONCRETE WALL

The development of a rigorous, yet conservative hazards analysis, based on the previously defined thermal criteria, requires that the thermal response of the concrete wall be characterized over a wide range of incident heat fluxes. The arrangement of the fire and concrete wall to be analyzed

is illustrated in Figure 2-1. A large fire plume, at a distance R, is assumed to emit thermal radiation uniformly in all directions. Some of this radiation is incident on the concrete surfaces of the power plant. Following the method of Parker,[4] a steady-state approach is taken whereby a target element of unit area dA is identified on the building surface. For a range of (constant) heat fluxes incident on the target area, it is desired to find the exposure times necessary to exceed the thermal criteria defined in Section 1.3. Since these criteria address both internal wall temperature rise, as well as surface erosion processes, a closed form analytic solution is not possible and numerical solution techniques must be used.

## 2.1 Wall Model

A planar, one-dimensional wall constructed of reinforced concrete is considered. The target element is taken to be 1 $m^2$, with a wall thickness of 0.61 m (2 feet). This corresponds to the wall thickness of a typical control building at a nuclear power plant, and is the thinnest of typical reinforced concrete walls for seismic- and tornado-rated structures. The internal structural rebars are neglected in this thermal wall model, as they constitute only a few percent of the volume of the wall and they run transverse to the direction of heat flow.

### 2.1.1 Concrete Thermal Properties

Cement-based materials undergo a series of decomposition processes at high temperatures,[6,7] and the usual assumptions of constant thermal properties may lead to appreciable errors in thermal diffusion calculations. To more accurately model the thermal response of concrete, Harmathy[5] has developed thermal property relationships for concrete materials which include the effects of latent heat absorption (heat of decomposition). Basically this method requires that the specific heat capacity of the concrete be expressed in the following form:

$$C_p = C_{pc} + C_{pHD} \qquad (2.1)$$

where $C_p$ is the total heat capacity, $C_{pc}$ is the caloric heat capacity, and $C_{pHD}$ is the effective heat capacity due to the absorption of latent heat (heat of decomposition).

The total volumetric heat capacity used in the present analysis is shown in Figure 2-2 as reproduced from Harmathy. The principal peaks of this curve are associated with the decomposition process. The dashed line indicates the approximate value for the volumetric heat capacity in the absence of any decomposition processes. Note that the

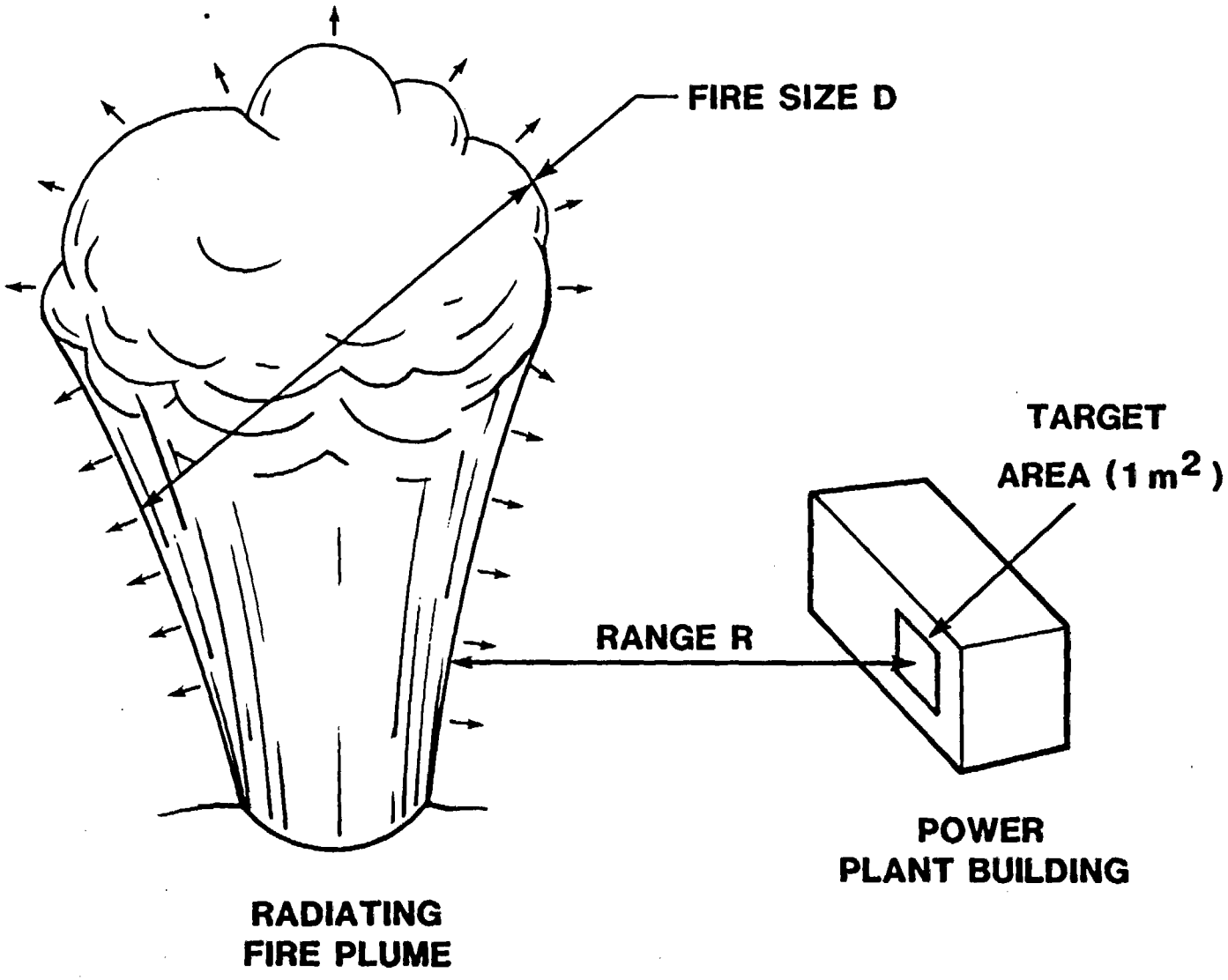


Figure 2-1. Thermal Hazard Posed by a Large Fire in the Vicinity of a Power Plant Structure

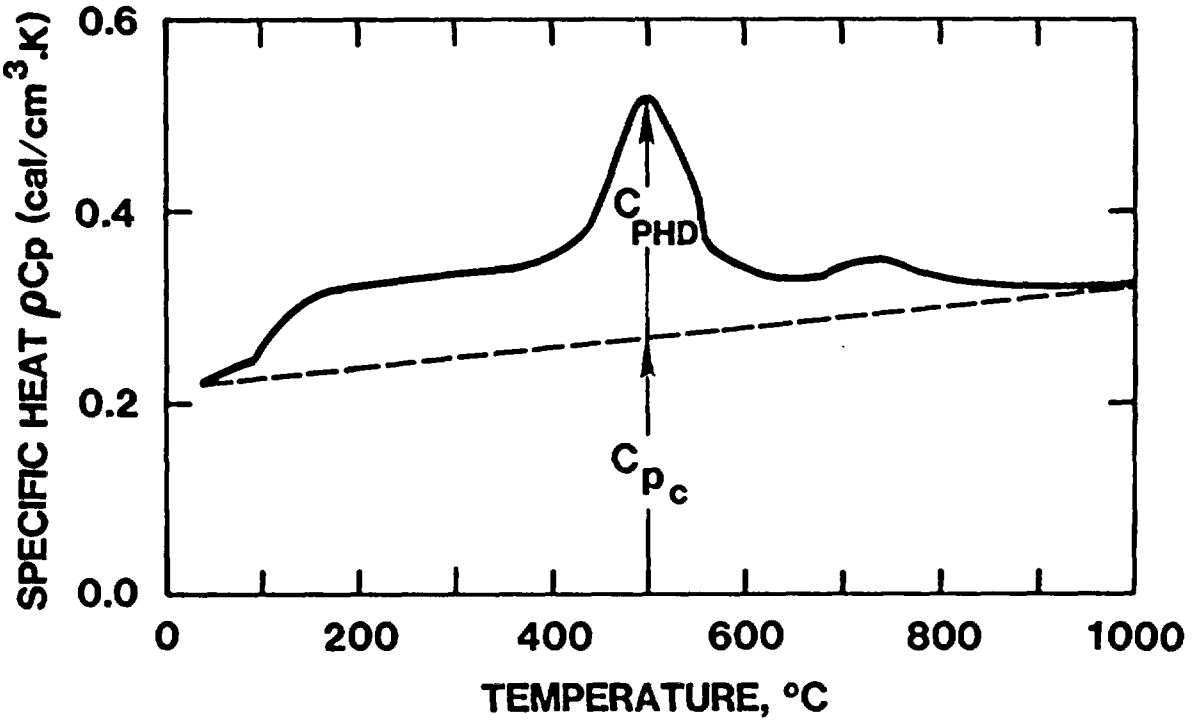


Figure 2-2. Thermal Properties for Concrete-Volumetric Specific Heat

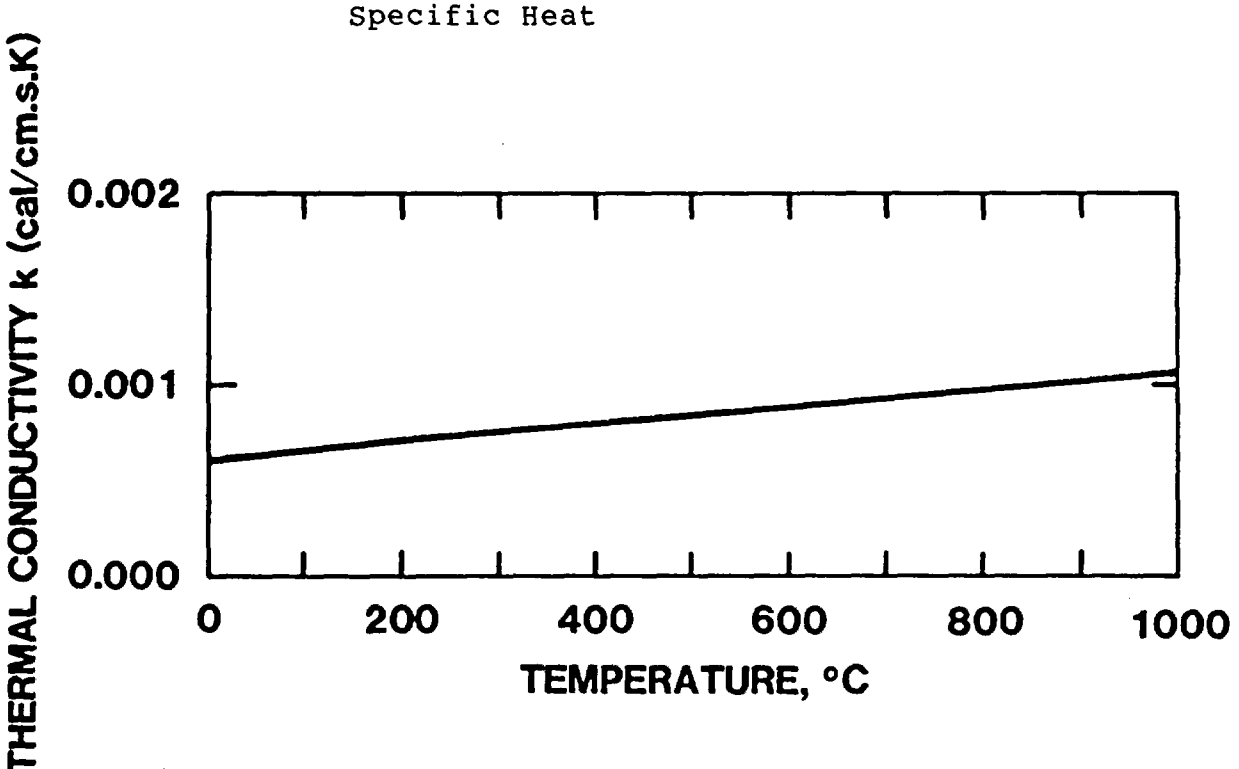


Figure 2-3. Thermal Properties for Concrete-Thermal Conductivity

heat capacity due to latent heat effects is a significant fraction of the total heat capacity, and thus cannot be ignored.

For the thermal conductivity, Harmathy developed governing relationships assuming the concrete to decompose as a multiphase solid mixture.[5] In general, the thermal conductivity of concrete is less affected by chemical composition than the heat capacity, as shown in Figure 2-3. Over a 1000°C temperature range, the thermal conductivity can be seen to change only moderately.

Neglecting thermal expansion effects, as well as changes in internal porosity, the density of concrete may be taken to be constant. The value for concrete density used in the present wall model was 1.7 $Mg/m^3$.

### 2.1.2 Surface Erosion Model

Since the thermal diffusivity for concrete is comparatively low ($\alpha \approx 6.9 \times 10^{-5}$ $m^2/s$ or 0.25 $m^2/hr$), the time scale governing heat conduction into the interior of the wall is large. Consequently, the principal effect of a large incident heat flux rate is to produce very large temperature gradients near the exposed surface. Should the wall temperature and the surface gradient become sufficiently large, a steady erosion-ablation process is established on the exterior surface. In the experiments conducted by Muir,[6] surface erosion rates for ablating concrete were measured for large values of radiant heat flux (640 to 1180 $kW/m^2$). Later, Chu[7] demonstrated that the surface erosion rate, $\delta$, could be correlated by the one-dimensional ablation expression for concrete

$$\delta = \frac{\int_0^t \exp q \, dt}{\rho[\bar{C}_p(T_a - T_o) + \Delta H_a]} \qquad (2.2)$$

where $T_a$ and $\Delta H_a$ are the effective ablation temperature and the effective latent heat of ablation, respectively. Correlation of Muir's concrete ablation data indicates that $T_a$ = 1350°C and $\Delta H_a = 3.08 \times 10^3$ J/g give good predictions of surface erosion depths as a function of exposure time.

### 2.1.3 Boundary Conditions

In the present wall model, the incident heat flux on the exposed surface was assumed to be independent of time. A surface absorptivity of 0.9 was assumed for the exterior

surface, with convective losses neglected. A natural convective coefficient of 5.7 $W/m^2C$ was assumed to be present on the interior surface; ie, at 0.61 m. The ambient temperature, as well as the initial temperature of the wall, was assumed to be 32°C (90°F).

## 2.2 Numerical Calculations

With the previously described wall model, numerical calculations were performed using the finite-difference heat conduction code, CINDA-3G.[8] Subroutines available in the code allowed the erosion-ablation process to be simulated in accordance with Equation 2.2. Thermal solutions were generated for values of incident heat flux ranging from 15 to 1400 $kW/m^2$.

In Figure 2-4, a typical time-temperature curve is shown at an internal location in the wall for an incident heat flux on the surface of 25 $kW/m^2$. The x-position in the wall is that pertaining to the first thermal criterion, the first rebar location at 0.15 m (0.5 ft). Solutions for three different values of exposure time are presented. Notice that as expected, the temperature history of the wall is identical for the three values of exposure time, up until the termination of the exposure. Due to thermal conduction in the wall, the maximum temperature at this location occurs approximately four hours after the termination of the exposure. For a given value of incident heat flux, the exposure time may be varied to determine the minimum exposure duration necessary to exceed any of the wall thermal criteria. In Figure 2-4, this result is exemplified by the solution for $t_{exp}$ = 8 hours. For this particular case, the maximum temperature just reaches the $T_{max}$ = 177°C criterion line. It may be concluded that for an incident flux of 25 $kW/m^2$, an exposure time of 8 hours is necessary to exceed the first thermal criterion.

When the value of the incident heat flux is sufficiently large, the temperature on the exterior surface of the wall increases until the effective ablation temperature is reached. An erosion front is established which propagates into the wall as the exposure time is increased. The desired solution is the time required to erode the first 0.076 m (0.25 ft) of the exposed surface, as specified in the second criterion. Results for this type of calculation are exemplified by the CINDA solutions shown in Figure 2-5. The temperature curves presented are those for an incident heat flux of 600 $kW/m^2$. The first curve, at $t_{exp}$ = 0.033 hours denotes the temperature distribution in the wall at the onset of erosion. Notice that the penetration of heat into the wall is relatively low, on the order of 0.025 m. Considering the low thermal diffusivity for concrete, this low value of thermal penetration is to be expected. For

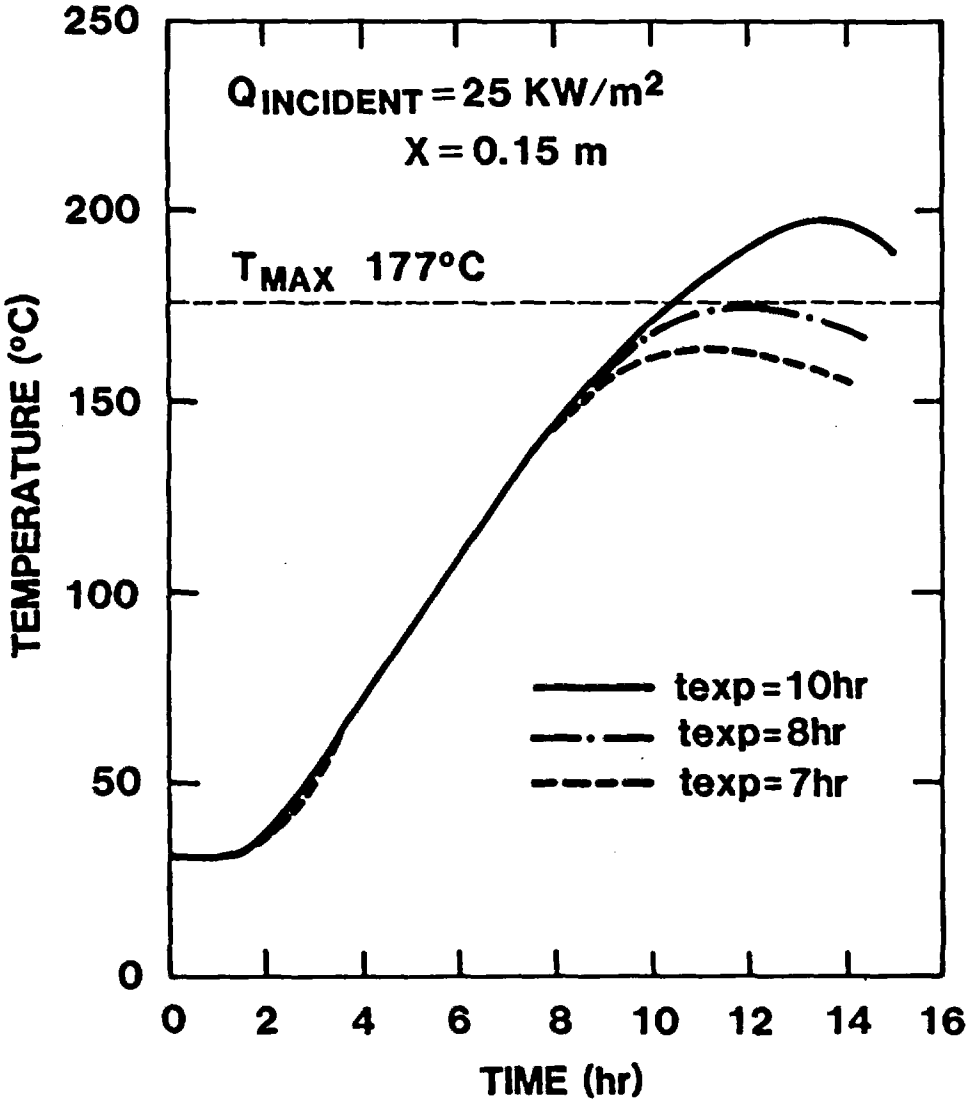


Figure 2-4. Typical Time-Temperature Curve at the 0.15 m Location

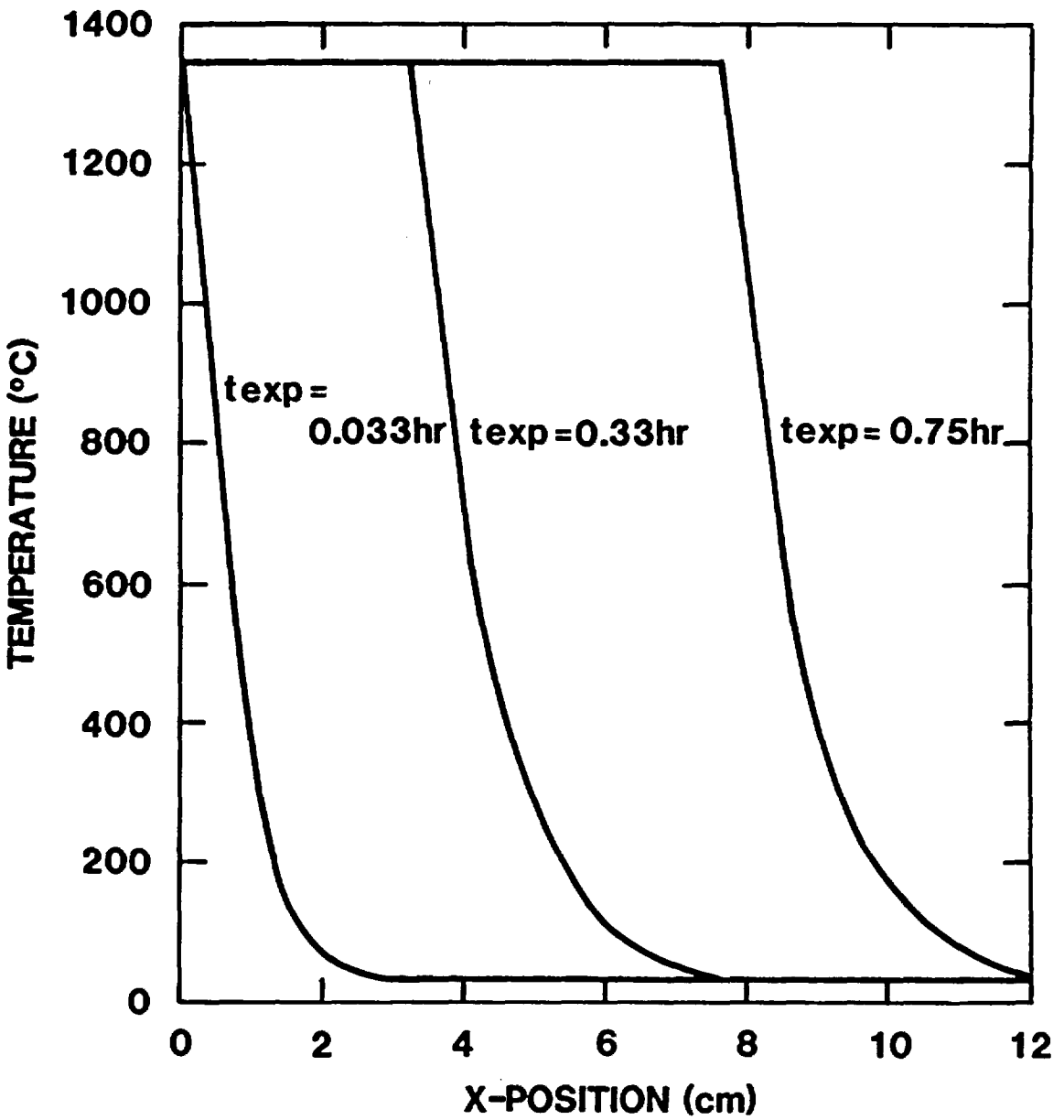


Figure 2-5. Position of Erosion Front as a Function of Exposure Time

increasing exposure time, the erosion front propagates through the wall with the incident thermal energy providing a source for the latent heat of ablation. At an exposure time of 0.75 hours, the erosion front reaches the 0.076-m location. The residual thermal energy present in the wall is insufficient to cause the temperature to reach 177°C at the 0.15-m location (to exceed criterion 1) due to surface cooling and the low thermal conductivity of concrete. Therefore, for an incident heat flux of 600 $kW/m^2$, an exposure time of more than 0.75 hours is required to exceed the erosion thermal criterion.

## 2.3 Wall Thermal Capacity

The calculations described above were repeated over a range of incident heat fluxes (15 to 1400 $kW/m^2$). The minimum exposure time necessary to exceed any one of the three previously defined thermal criteria was determined. Tabulated values for the incident heat flux and the required exposure time are presented in Table 2-1. It is evident from these values that the onset of erosion occurs at an incident thermal flux of approximately 350 to 400 $kW/m^2$. Another important conclusion that may be drawn from these results is that criterion 3 cannot be exceeded without first exceeding criterion 1 (see Section 1.3). That is, by the time the heat conducts to the interior surface of the wall (at 0.61 m), the temperature at the first rebar will have exceeded criterion 1 for all cases.

In Figure 2-6, the tabulated values appear in graphical form.

Notice that for the low values of incident flux, criterion 1 was exceeded, while for high values of the incident flux, criterion 2 was exceeded. Joining these two regimes are solutions for which the conduction criterion was exceeded with the onset of ablation occurring at the exposed surface. The inflection in the curve is a result of the heat absorbed in the erosion process. Thus, the results for an incident flux of 350 $kW/m^2$ indicate a slightly longer exposure time is necessary to exceed criterion 1 than for 300 $kW/m^2$ due to the absorption of latent heat.

# 3.0 FIRE MODELING

For the purpose of estimating the vulnerability of nuclear power plants to large external fires, a simple fire model for estimating the radiative thermal output of the fire is developed. The results are conservative so that the vulnerability estimates are bounds. The simplicity of the model arises from the use of macroscopically observable quantities (eg, heat of combustion and surface heat flux).

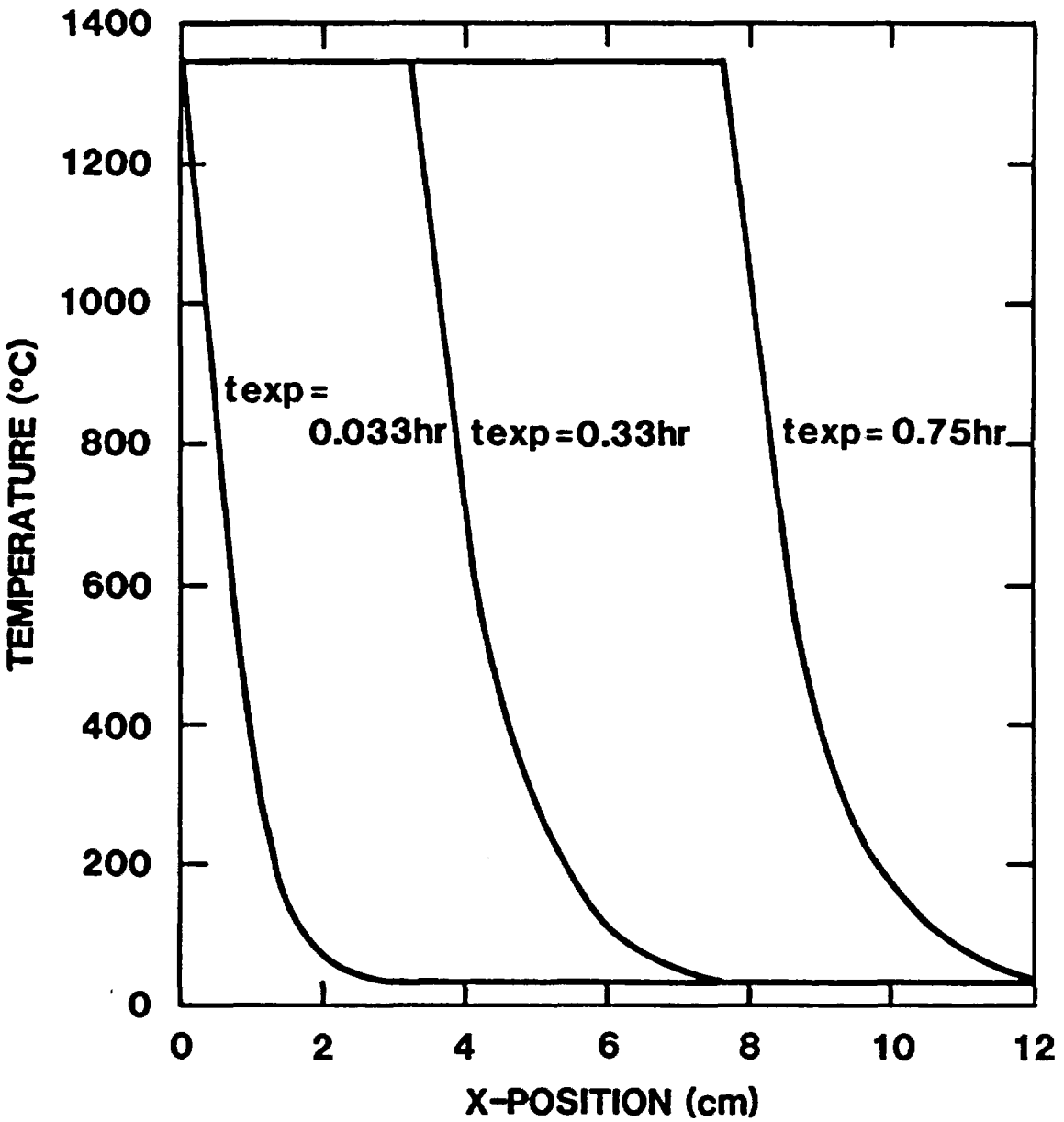


Figure 2-5. Position of Erosion Front as a Function of Exposure Time

increasing exposure time, the erosion front propagates through the wall with the incident thermal energy providing a source for the latent heat of ablation. At an exposure time of 0.75 hours, the erosion front reaches the 0.076-m location. The residual thermal energy present in the wall is insufficient to cause the temperature to reach 177°C at the 0.15-m location (to exceed criterion 1) due to surface cooling and the low thermal conductivity of concrete. Therefore, for an incident heat flux of 600 $kW/m^2$, an exposure time of more than 0.75 hours is required to exceed the erosion thermal criterion.

## 2.3 Wall Thermal Capacity

The calculations described above were repeated over a range of incident heat fluxes (15 to 1400 $kW/m^2$). The minimum exposure time necessary to exceed any one of the three previously defined thermal criteria was determined. Tabulated values for the incident heat flux and the required exposure time are presented in Table 2-1. It is evident from these values that the onset of erosion occurs at an incident thermal flux of approximately 350 to 400 $kW/m^2$. Another important conclusion that may be drawn from these results is that criterion 3 cannot be exceeded without first exceeding criterion 1 (see Section 1.3). That is, by the time the heat conducts to the interior surface of the wall (at 0.61 m), the temperature at the first rebar will have exceeded criterion 1 for all cases.

In Figure 2-6, the tabulated values appear in graphical form.

Notice that for the low values of incident flux, criterion 1 was exceeded, while for high values of the incident flux, criterion 2 was exceeded. Joining these two regimes are solutions for which the conduction criterion was exceeded with the onset of ablation occurring at the exposed surface. The inflection in the curve is a result of the heat absorbed in the erosion process. Thus, the results for an incident flux of 350 $kW/m^2$ indicate a slightly longer exposure time is necessary to exceed criterion 1 than for 300 $kW/m^2$ due to the absorption of latent heat.

# 3.0 FIRE MODELING

For the purpose of estimating the vulnerability of nuclear power plants to large external fires, a simple fire model for estimating the radiative thermal output of the fire is developed. The results are conservative so that the vulnerability estimates are bounds. The simplicity of the model arises from the use of macroscopically observable quantities (eg, heat of combustion and surface heat flux).

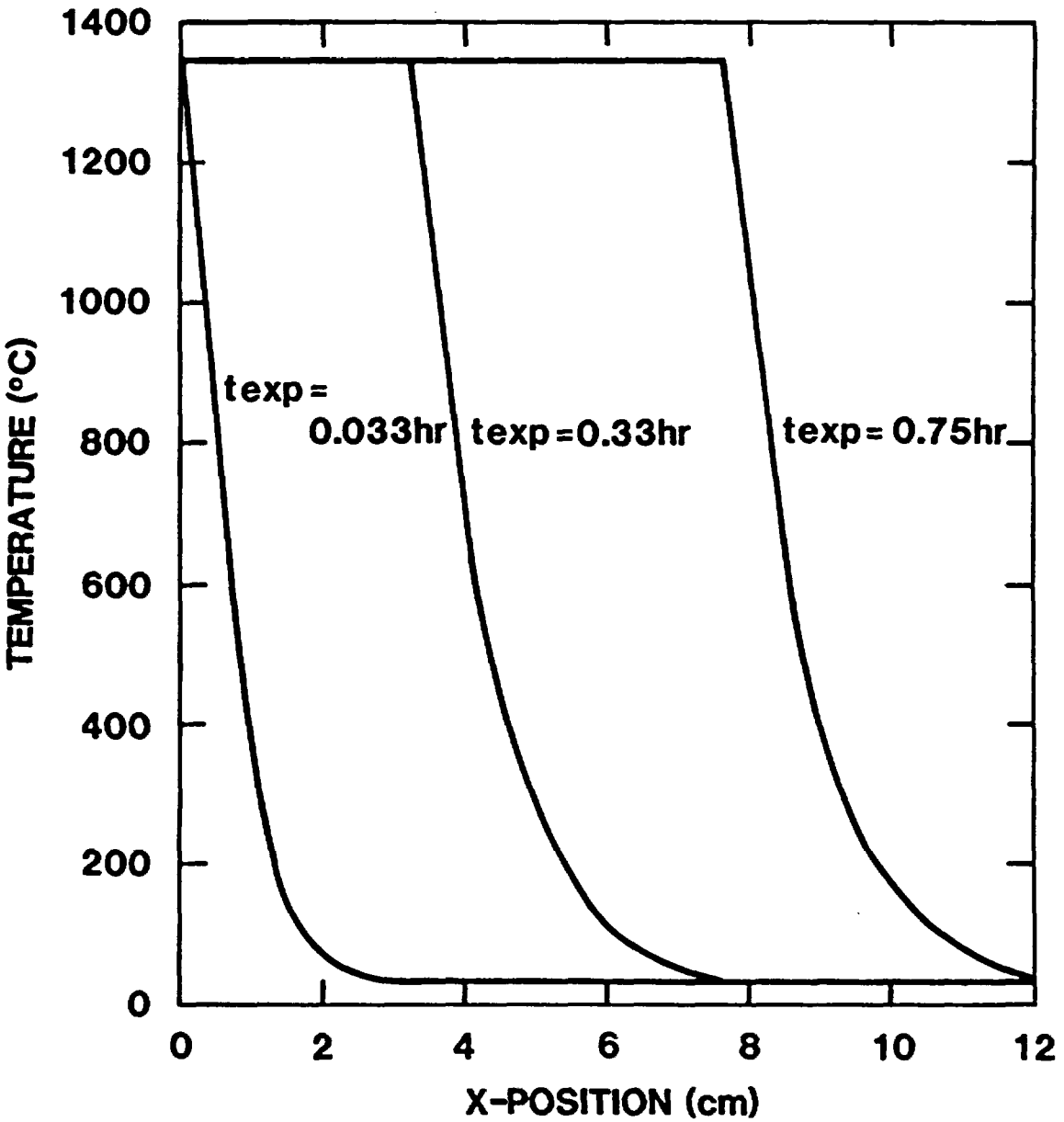


Figure 2-5. Position of Erosion Front as a Function of Exposure Time

increasing exposure time, the erosion front propagates through the wall with the incident thermal energy providing a source for the latent heat of ablation. At an exposure time of 0.75 hours, the erosion front reaches the 0.076-m location. The residual thermal energy present in the wall is insufficient to cause the temperature to reach 177°C at the 0.15-m location (to exceed criterion 1) due to surface cooling and the low thermal conductivity of concrete. Therefore, for an incident heat flux of 600 $kW/m^2$, an exposure time of more than 0.75 hours is required to exceed the erosion thermal criterion.

## 2.3 Wall Thermal Capacity

The calculations described above were repeated over a range of incident heat fluxes (15 to 1400 $kW/m^2$). The minimum exposure time necessary to exceed any one of the three previously defined thermal criteria was determined. Tabulated values for the incident heat flux and the required exposure time are presented in Table 2-1. It is evident from these values that the onset of erosion occurs at an incident thermal flux of approximately 350 to 400 $kW/m^2$. Another important conclusion that may be drawn from these results is that criterion 3 cannot be exceeded without first exceeding criterion 1 (see Section 1.3). That is, by the time the heat conducts to the interior surface of the wall (at 0.61 m), the temperature at the first rebar will have exceeded criterion 1 for all cases.

In Figure 2-6, the tabulated values appear in graphical form.

Notice that for the low values of incident flux, criterion 1 was exceeded, while for high values of the incident flux, criterion 2 was exceeded. Joining these two regimes are solutions for which the conduction criterion was exceeded with the onset of ablation occurring at the exposed surface. The inflection in the curve is a result of the heat absorbed in the erosion process. Thus, the results for an incident flux of 350 $kW/m^2$ indicate a slightly longer exposure time is necessary to exceed criterion 1 than for 300 $kW/m^2$ due to the absorption of latent heat.

# 3.0 FIRE MODELING

For the purpose of estimating the vulnerability of nuclear power plants to large external fires, a simple fire model for estimating the radiative thermal output of the fire is developed. The results are conservative so that the vulnerability estimates are bounds. The simplicity of the model arises from the use of macroscopically observable quantities (eg, heat of combustion and surface heat flux).

TABLE 2-1

Tabulated Results of Wall Response Analysis

| Incident Heat Flux ($kW/m^2$) | Exposure Time (hours) | Criterion Bound |
|---|---|---|
| 15 | 11.6 | 1 |
| 25 | 8.1 | 1 |
| 50 | 4.95 | 1 |
| 100 | 3.15 | 1 |
| 200 | 2.03 | 1 |
| 300 | 1.65 | 1 |
| 350 | 1.70 | 1 |
| 400 | 1.79 | 1 |
| 450 | 1.53 | 1 |
| 500 | 1.15 | 2 |
| 600 | 0.74 | 2 |
| 700 | 0.55 | 2 |
| 800 | 0.44 | 2 |
| 900 | 0.37 | 2 |
| 1000 | 0.32 | 2 |
| 1200 | 0.25 | 2 |
| 1400 | 0.20 | 2 |

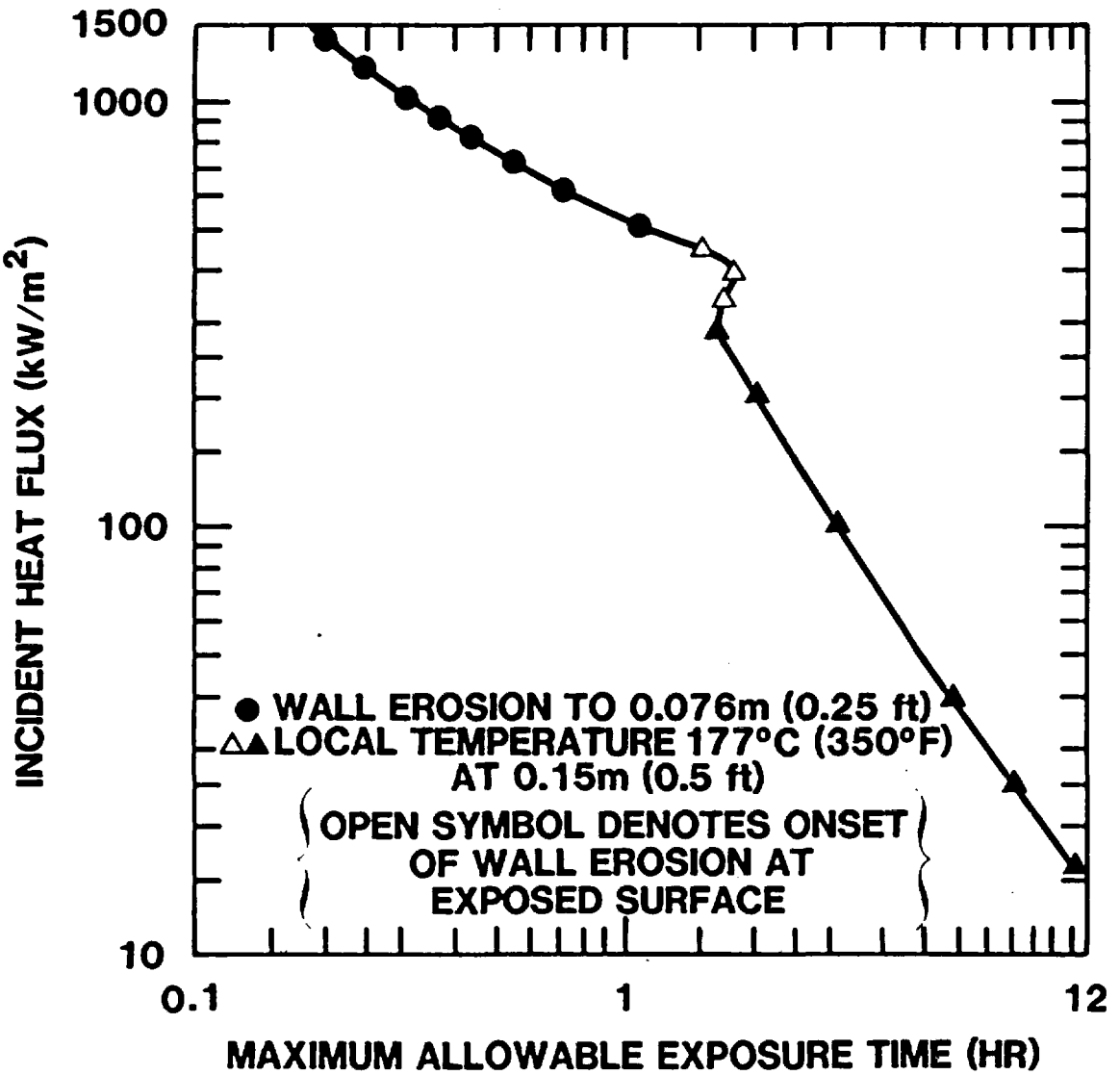


Figure 2-6. Incident Heat Flux Versus Maximum Allowable Exposure Time

Details of combustion processes and fire dynamics are included to the extent that they affect the macroscopic characteristics of the fire.

The model is described in three sections:

Radiant Energy
Flame Area
Flame Shape and View Factor.

In the first section, an estimate is made for the fraction of the total available energy leaving the flame by radiation. The second describes a method for estimating the size of the flame, and hence the radiative area which would irradiate the target. The last section uses shape factor relationships to predict the thermal flux incident upon the target area as a function of range.

## 3.1 Radiant Energy

The large fires under consideration burn as turbulent diffusion flames. The fuel (as a vapor) enters the flame zone and mixes with entrained air. Due to the turbulent and nonuniform mixing, there is both incomplete combustion and excess air entrained in the plume. The combustion products (at their elevated temperatures) radiate thermal energy to the surrounding environment. This results in an average flame temperature which is lower than the adiabatic flame temperature. The adiabatic flame temperature would be observed if the fuel vapor were premixed with the proper amount of oxygen and burned stoichiometrically with no heat loss to the surroundings. The difference between the adiabatic and the actual flame temperature (for the stoichiometric mixture) is then primarily a measure of the radiant energy output of the flame. The remaining energy leaves the flame zone as hot combustion products at the (actual) flame temperature.

Assuming the combustion volume to have uniform characteristics, the rate at which energy is emitted as radiation from the burning plume can be expressed as follows:

$$P_R = M_F[\eta\Delta H_C - (T_f - T_a)(\eta S(1 + \chi)C_{pa} + C_{pf})]/10^3 \quad (3.1)$$

where

$P_R$ = total radiated power (kW)

$M_F$ = fuel flow rate or consumption rate (kg/s)

$\eta$ = fraction of fuel burned ($0 \leq \eta \leq 1$)

$\Delta H_C$ = heat of combustion of fuel (J/kg)

$T_f$ = flame temperature of combustion products (K)

$T_a$ = ambient air temperature (K)

$\chi$ = fraction of excess air ( $\chi$ = 0 for stoichiometric combustion)

S = stoichiometric air/fuel ratio (kg-air/kg-fuel)

$C_{pa}$ = mean heat capacity of air (J/kgK)

$C_{pf}$ = mean heat capacity of fuel vapor (J/kgK)

Ignoring minor heat losses such as convection and molecular dissociation, the radiated energy is simply the total energy produced, less that needed to heat the entering fuel vapor and air to the flame temperature. For this study, it will be conservatively assumed that all of the fuel burns ( $\eta$ = 1). It is noted that if $T_f$ equals the adiabatic flame temperature, then $P_R$ is ideally zero.

The fraction of excess air, $\chi$ , entrained in the burning plume is relatively difficult to measure and has been correlated from experimental data only for small-scale fires. Values reported in the literature range from 2 to as high as 10, for small turbulent fires on the order of a few meters in height.[20,21,22] Data for large-scale fires (eg, hundreds of meters in height) is lacking. For this study, a conservative value of 0.25 will be used.

## 3.2 Flame Area

An estimate of the surface area, and hence the size of the burning plume, can be made from knowledge of the specific emissive power (per unit area) at the flame surface. For large pool type fires (eg, gasoline, liquid petroleum products), measured values for the emission power range from 62 to 174 $kW/m^2$. The range of heat fluxes from the surface of large NG and LPG fireballs is 120 to 500 $kW/m^2$.[19] Much of the difference in (per area) thermal output between these two types of fires is due to variations in a number of fire characteristics, including fuel type, mean flame temperature, and optical properties of the combustion products. For the purposes of conservatively estimating flame surface area, and hence the size of the fire plume, a value for the specific emissive power should be selected that is from the lower end of the range. This will then give a bounding estimate for the flame surface area. For this study, a specific emissive power $P_{SL}$, of 75 $kW/m^2$ for pool fires and 150 $kW/m^2$ for fireballs will be used for estimating flame area.

There is very little experimental data on the plume size for the very large fires for which the fuel burning rate is

well characterized. In Chapter 4 an example calculation for a 6" NG pipeline provides a comparison with flame sizes obtained during a series of fire extinguishing tests. Based on this data, a more realistic estimate of the flame size might be obtained by using a central estimate for the specific emitted power per unit area, rather than a lower bound (conservative) estimate as described above. The difference in specific powers for lower bound and central estimates is about a factor of 2, while the difference in flame area estimates in Section 4.3 for our method and Reference 16 is about a factor of 4.

In summary, the effective emitting surface area $A_F$ of the fire plume is:

$$A_F = P_R/P_{SL} \tag{3.2}$$

where $P_R$ is given by Equation 3.1. From this and an assumed flame shape (sphere, upright circular cylinder, etc), the size of the flame can then be estimated.

## 3.3 Flame Shape and View Factor

The previous sections considered the thermal output from the flame and the resultant flame surface area. The thermal energy incident upon a target area located at a range R from the flame is determined by the radiative output of the fire source and the view factor between the flame and target:[9]

$$Q_i = P_{SU}TA_FF_{F-T} \tag{3.3}$$

where

$Q_i$ = thermal power received by target ($kW/m^2$).

$P_{SU}$ = specific thermal power emitted from the surface of the flame, upper bound estimate ($kW/m^2$).

$T$ = transmissivity of the atmosphere.

$A_F$ = flame surface area ($m^2$).

$F_{F-T}$ = view factor -- flame to target.

The target is assumed to have unit area; eg, 1 $m^2$.

Since $Q_i$ should be a conservative estimate of the radiative flux incident upon the target, the values for $P_{SU}$ for pool fires and fireballs should be selected from the upper end of the observed ranges. Using the ranges of values cited in Section 3.2, and based on a review of the specific experimental conditions cited in the literature,

specific emissive powers of 150 $kW/m^2$ for pool fires and 350 $kW/m^2$ for fireballs will be used for $P_{SU}$.

The reciprocity relationship between the emitting (flame) and receiving (target) areas can be expressed as:

$$A_F F_{F-T} = A_T F_{T-F} \tag{3.4}$$

Since the target area is actually an unspecified unit area on a building, these two expressions can be combined to give the thermal energy received by the target per unit area $Q_i (kW/m^2)$:

$$Q_i = P_{SU} {}^T F_{T-F} \tag{3.5}$$

Analytic expressions for the view factor $F_{T-F}$ have been developed extensively in the literature.[9] One of the simplest relationships describes the view factor between a differential element and a sphere, with the element oriented perpendicular to a radial line:

$$F_{T-F} = \left( \frac{D}{D + 2R} \right)^2 \tag{3.6}$$

where

D = diameter of sphere

R = range from the surface of the sphere to the target.

A spherical shape is probably most appropriate for a fireball.

For high pressure pipeline fires, the shape can be approximated by a vertical circular cylinder. The analytic expression for the view factor is very complex.[9] It is instructive to compare the view factor for a sphere and cylinder as a function of range. For this comparison, the two objects have the same total surface area. A relatively conservative aspect ratio (length/diameter) of 2 was chosen for the cylinder. The target area is conservatively assumed to be offset from the center of the cylinder and not from one end. The view factors for two sphere sizes (200 m and 400 m diameters), and the corresponding equivalent cylinders, are shown in Figure 3-1. Also shown are the view factors for plane discs having the same diameter as the spheres. While the view factor for a sphere would tend to underestimate that for a cylinder, the factor for a plane disc would bound the values for both spheres and cylinders, without being unduly conservative, especially for ranges above 1000 m. For this work, the view factor for a plane disc will be used:

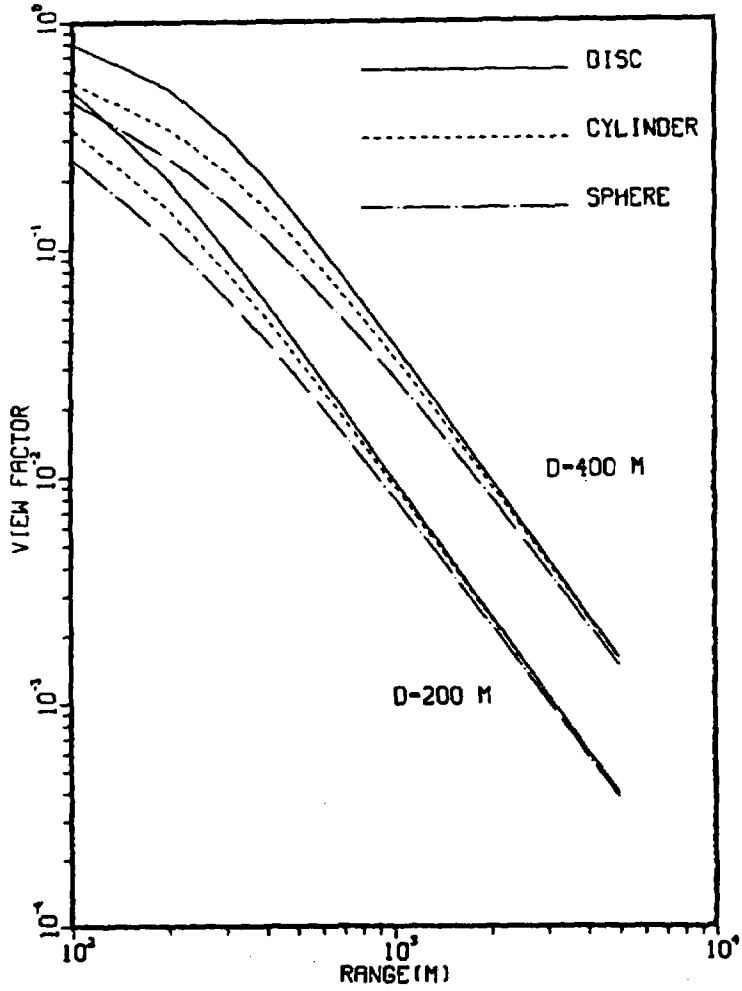


Figure 3-1. Flame-to-Target View Factors

$$F_{T-F} = \left(\frac{D^2}{D^2 + 4R^2}\right) \tag{3.7}$$

where D, the diameter of the disc, is the same as the diameter of the spherical flame:

$$A_F = \pi D^2 = P_R/P_{SL} \tag{3.8}$$

Remember that $P_{SL}$ is a lower bound estimate of the thermal power emitted from the surface of the flame.

The principal reduction of the thermal flux with distance is the shape factor developed above. Having a lesser effect is the reduction due to absorption in the intervening atmosphere, principally by water vapor. Normal levels of dust do not significantly contribute to the attenuation as compared to water vapor. For LNG flames, the transmissivity T of the atmosphere as a function of path length for several relative humidities is shown in Figure 3-2.[10,11] The use in an analysis of the upper curve would almost always be conservative, since the actual transmissivity would be less.

## 3.4 Incident Thermal Energy

Expressions have been developed in the previous sections for estimating the radiative flux incident upon a target area from large hydrocarbon fires. The thermal energy incident upon the target is given by

$$Q_i = P_{SU}TD^2/(D^2 + 4R^2). \tag{3.9}$$

Since each step in the analysis is conservative, $Q_i$ is an upper bound estimate for the radiative thermal flux incident on a target.

## 3.5 Fuel Flow Rates

The application of the previously developed models for estimating thermal output of typical large fires requires knowledge of fuel characteristics and an estimate of the fuel consumption rate. This latter estimate is dependent on accident conditions; eg, fuel release rate, fuel consumption rate, air entrainment rate, etc, which are very difficult to quantify. In practice, the fuel discharge rate will probably be different than the burning rate or consumption rate by the fire, especially at the beginning and termination of the fire. Under a steady-state approximation, the consumption or burning rate is the same as the discharge rate from the tank or pipe. This steady-state discharge rate can be estimated from conditions known prior to the accident

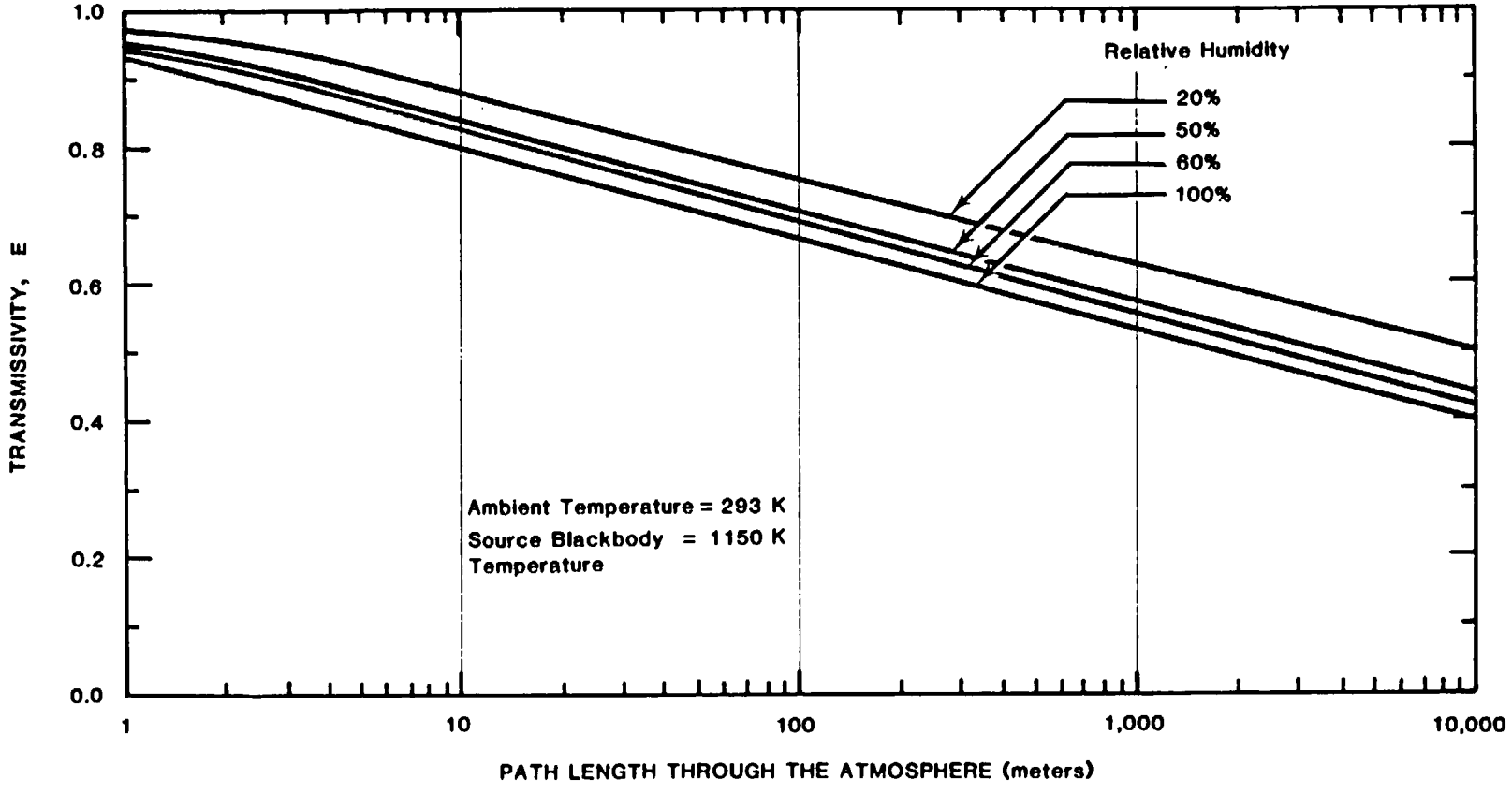


Figure 3-2. Atmospheric Transmissivity as a Function of Relative Humidity[10,11]

(pressure, level in the tank, etc) and an assumed value for discharge area. This obviates the need for detailed information describing the fire dynamics of a particular accident situation.

In the following two sections, methods for estimating fuel flow rates from a liquid fuel tank and a high-pressure pipeline are presented. The tank model is time-dependent, while the pipeline analysis uses an approximate, steady-state solution.

### 3.5.1 Flow From a Tank

Consider a tank discharging a liquid fuel through an opening of area A. For simplicity, the tank is assumed to have a constant cross-sectional area S as shown.

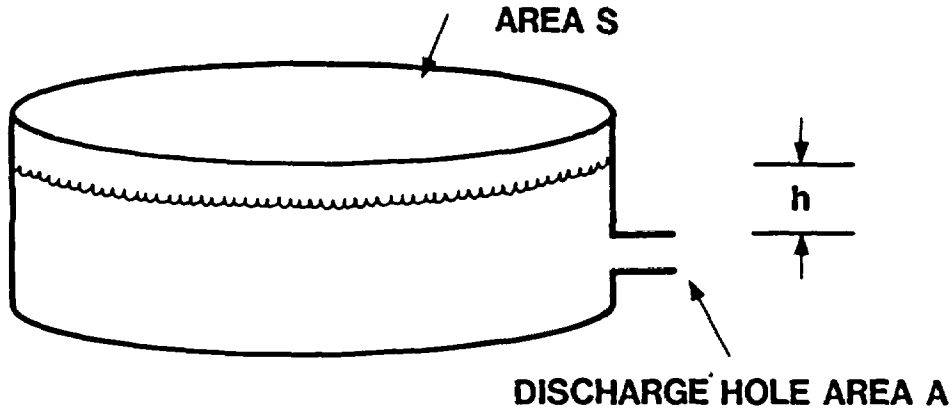


The discharge mass flow rate $M_F$ is given by:[12]

$$M_F = \rho V A \qquad (3.10)$$

where $\rho$ is the density of the fuel, and V is the discharge velocity. Application of Bernoulli's principle gives

$$V = C\sqrt{2gh} \qquad (3.11)$$

where C is the orifice flow coefficient (typical value 0.6). Developing a solution for h, the level of the fuel in the tank, as a function of time and substituting gives a linearly decreasing function for $M_F$:

$$M_F = \rho A C\sqrt{2gh_i} - \frac{\rho g C^2 A^2 t}{S} \qquad (3.12)$$

where $h_i$ is the initial height of the fuel in the tank relative to the discharge opening. Note that the initial flow rate (t = o) is directly proportional to the discharge area. The time required for the tank to drain is given by:

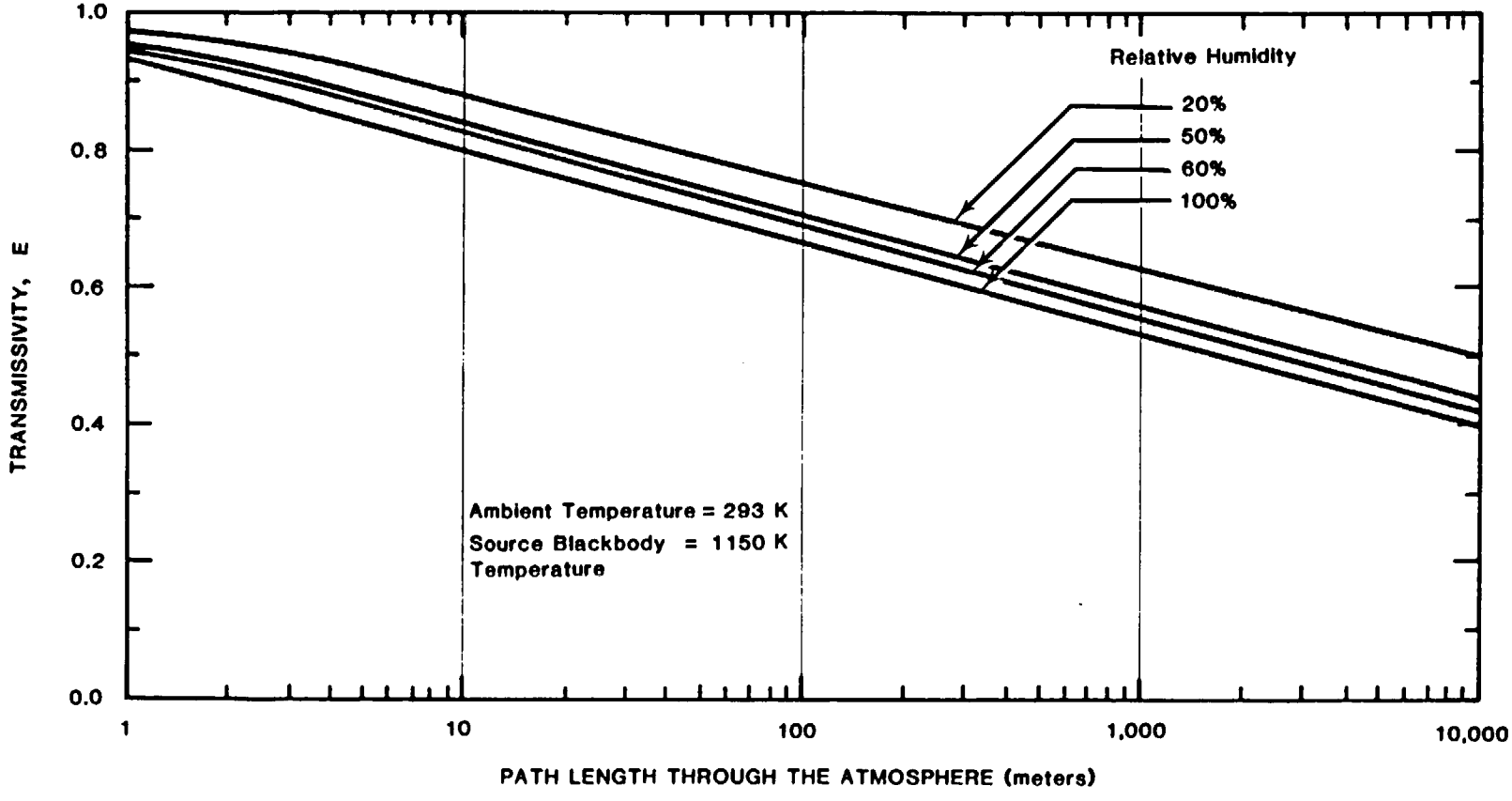


Figure 3-2. Atmospheric Transmissivity as a Function of Relative Humidity[10,11]

(pressure, level in the tank, etc) and an assumed value for discharge area. This obviates the need for detailed information describing the fire dynamics of a particular accident situation.

In the following two sections, methods for estimating fuel flow rates from a liquid fuel tank and a high-pressure pipeline are presented. The tank model is time-dependent, while the pipeline analysis uses an approximate, steady-state solution.

### 3.5.1 Flow From a Tank

Consider a tank discharging a liquid fuel through an opening of area A. For simplicity, the tank is assumed to have a constant cross-sectional area S as shown.

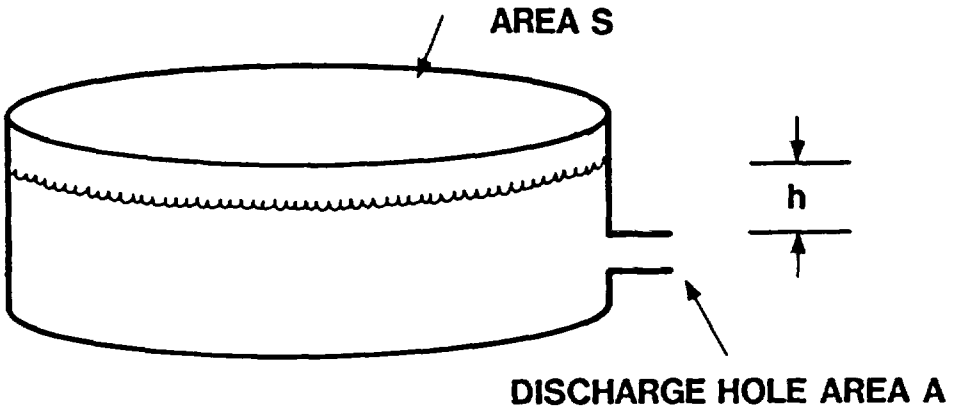


The discharge mass flow rate $M_F$ is given by:[12]

$$M_F = \rho V A \qquad (3.10)$$

where $\rho$ is the density of the fuel, and V is the discharge velocity. Application of Bernoulli's principle gives

$$V = C\sqrt{2gh} \qquad (3.11)$$

where C is the orifice flow coefficient (typical value 0.6). Developing a solution for h, the level of the fuel in the tank, as a function of time and substituting gives a linearly decreasing function for $M_F$:

$$M_F = \rho A C \sqrt{2gh_i} - \frac{\rho g C^2 A^2 t}{S} \qquad (3.12)$$

where $h_i$ is the initial height of the fuel in the tank relative to the discharge opening. Note that the initial flow rate (t = o) is directly proportional to the discharge area. The time required for the tank to drain is given by:

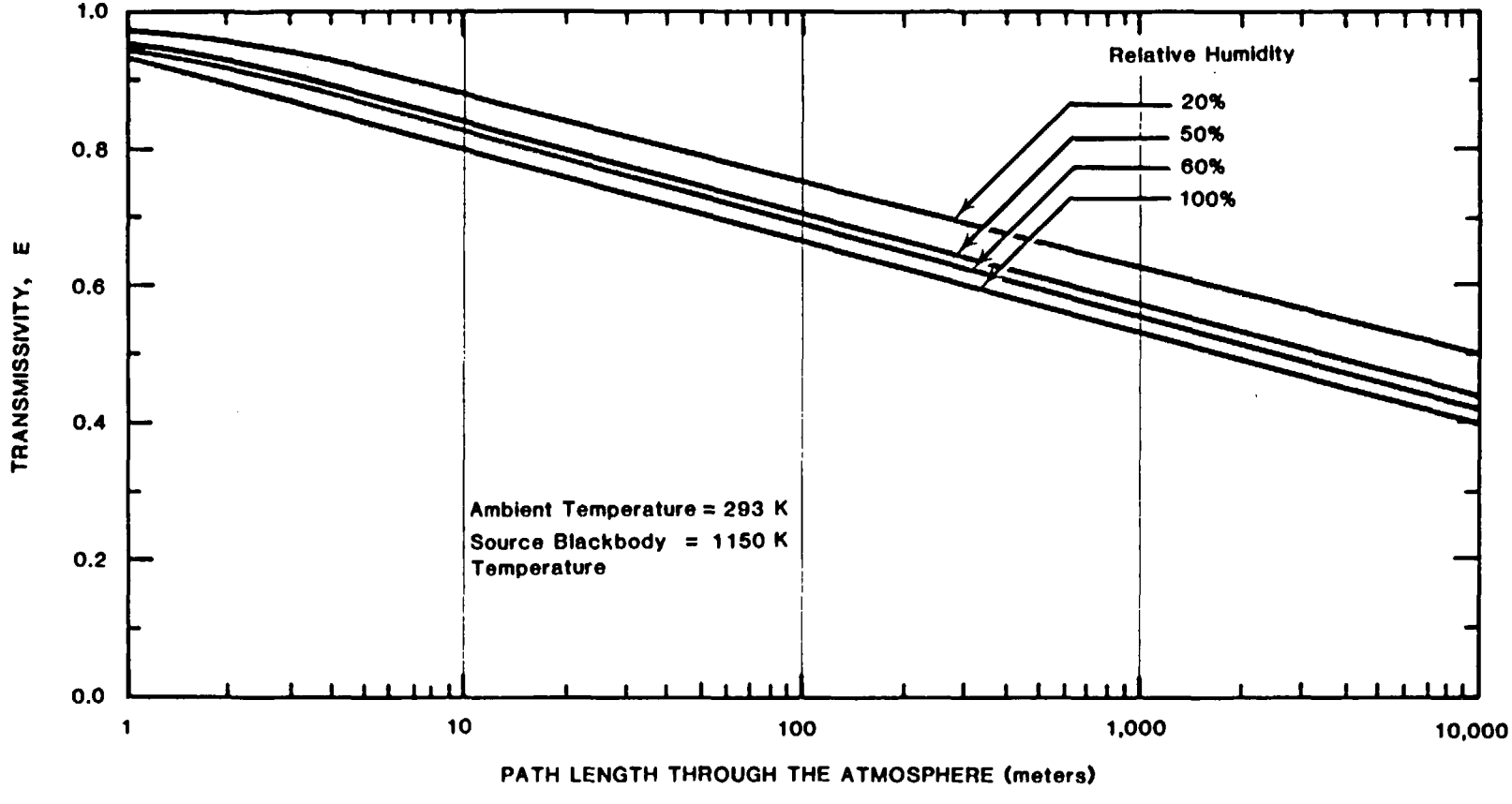


Figure 3-2. Atmospheric Transmissivity as a Function of Relative Humidity[10,11]

(pressure, level in the tank, etc) and an assumed value for discharge area. This obviates the need for detailed information describing the fire dynamics of a particular accident situation.

In the following two sections, methods for estimating fuel flow rates from a liquid fuel tank and a high-pressure pipeline are presented. The tank model is time-dependent, while the pipeline analysis uses an approximate, steady-state solution.

### 3.5.1 Flow From a Tank

Consider a tank discharging a liquid fuel through an opening of area A. For simplicity, the tank is assumed to have a constant cross-sectional area S as shown.

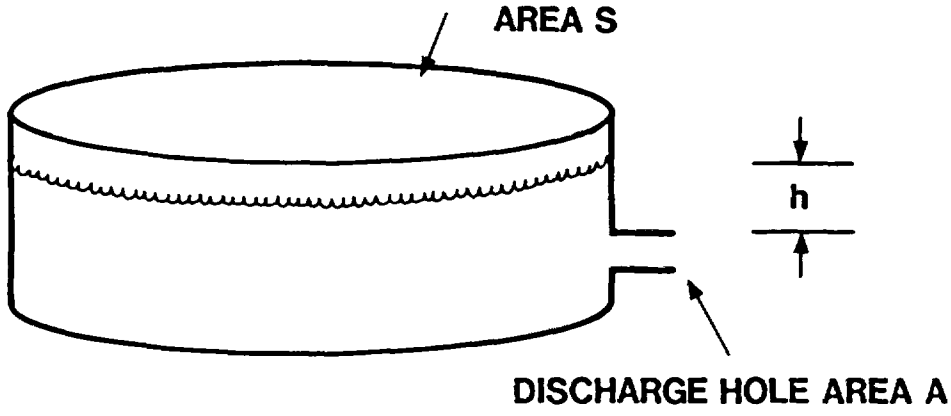


The discharge mass flow rate $M_F$ is given by:[12]

$$M_F = \rho V A \qquad (3.10)$$

where $\rho$ is the density of the fuel, and V is the discharge velocity. Application of Bernoulli's principle gives

$$V = C\sqrt{2gh} \qquad (3.11)$$

where C is the orifice flow coefficient (typical value 0.6). Developing a solution for h, the level of the fuel in the tank, as a function of time and substituting gives a linearly decreasing function for $M_F$:

$$M_F = \rho A C \sqrt{2gh_i} - \frac{\rho g C^2 A^2 t}{S} \qquad (3.12)$$

where $h_i$ is the initial height of the fuel in the tank relative to the discharge opening. Note that the initial flow rate (t = o) is directly proportional to the discharge area. The time required for the tank to drain is given by:

$$t_D = \frac{S}{CA} \left(\frac{2h_i}{g}\right)^{1/2} \qquad (3.13)$$

### 3.5.2 Discharge From a High-Pressure Pipeline

High-pressure pipelines are used principally for the transport of large quantities of methane (natural gas, NG), and to a lesser extent, liquified petroleum gas (propane-butane). This study will consider only NG pipelines, whose sizes range up to 1.1 m (3-1/2') diameter, with operating pressures from 4.8 to 6.9 MPa (700 to 1000 psi)[18] and normal flow velocities about 10 to 15 m/s (25 to 35 mph).

Breaks in such pipelines produce choked flow, in which the discharge velocity is near sonic and the mass flow rate is relatively independent of the downstream (atmospheric) pressure. In Appendix A an approximate steady-state analysis is developed for the blowdown of a high-pressure, natural gas pipeline, in which the long pipe acts as the reservoir and as a flow restrictor (through friction). Since such a complex model is relatively difficult to use, the detailed calculations are presented in Appendix A and a range of blowdown flow rates are summarized for various pipeline diameters in Table 3-1. Also listed for each size are the estimated flame heights, based on correlations from Reference A3 for turbulent diffusion flames, and equivalent spherical flame diameters, based on this work.

TABLE 3-1

Maximum Discharge Flow Rates for NG Transmission Pipelines

| Pipeline Diameter meters (feet) | Mass Flow Rate (kg/s) | Flame Height (m) | Equivalent Spherical Diameter (m) |
|---|---|---|---|
| .15 (0.5) | 14-25 | 56-61 | 27-36 |
| .30 (1.0) | 80-140 | 110-140 | 65-84 |
| .45 (1.5) | 270-280 | 170-210 | 110-140 |
| .61 (2.0) | 520-810 | 240-290 | 160-200 |
| .91 (3.0) | 1400-2100 | 370-440 | 270-330 |
| 1.07 (3.5) | 2000-3200 | 430-530 | 320-400 |

## 4.0 EXAMPLE CALCULATIONS

For illustrative purposes, three example fire accident scenarios are analyzed for the purpose of predicting the resultant heat flux as a function of range and maximum allowable exposure duration. The first is a 0.91 m (3') diameter high-pressure, natural gas pipeline with an assumed hole diameter equal to the pipeline size. The second is a large gasoline storage tank with a 1 $m^2$ diameter discharge hole area. The third analysis considers a 0.15 m (1/2') diameter high-pressure, NG pipeline and provides a flame size comparison with some experimental data.

### 4.1 High-Pressure Natural Gas Pipeline

Consider the discharge from a 0.91 m (3') diameter natural gas transmission line exhausting through a 0.91 m (3') circular hole. The standard operating pressure is assumed to be 69 MPa (1000 psig). From Appendix A, the mass flow rate ranges from 1400 to 2100 kg/s; an average value of 1700 kg/s will be used for $M_F$. The radiated power $P_R$ obtained assuming complete combustion is given by Equation 3.1:

$$P_R = M_F[\eta\Delta H_C - (T_f - T_a)( S(1 + X)C_{pa} + C_{pf})]/10^3$$

where

$\eta$ = fraction of fuel burned

= 1.

$\Delta H_C$ = heat of combustion of fuel

= 2.13 x $10^5$ cal/mole[13]

= 5.6 x $10^7$ J/kg

$T_f$ = flame temperature or temperatures of combustion products

= 1500 K[14]

$T_a$ = initial air temperature

= 300 K

X = fraction of excess air

= 0.25

S = stoichiometric air/fuel ratio

$= 17$[13]

$C_{pa}$ = mean heat capacity of air

$= 1150$ J/kg K[13]

$C_{pf}$ = mean heat capacity of fuel

$= 2200$ J/kg K[13]

Substituting, we have:

$$P_R = (1700 \text{ kg/s})\left\{(5.6 \times 10^7) - 1500 - 300) \times [(17.2)(1 + 0.25)(1150 \text{ J/kg}) + (2200 \text{ J/kg})]\right\}/10^3$$

$$= (1700 \text{ kg/s})\left\{(5.6 \times 10^7 \text{ J/kg}) - (3.2 \times 10^7 \text{ J/kg})\right\}/10^3$$

$$= 4.1 \times 10^7 \text{ kW}$$

The intermediate line above shows that about 60 percent of the theoretically available energy is used to heat up the fuel and entrained air.

Using a surface emittance of 150 kW/m$^2$ from Section 3.2 gives a surface area of $2.7 \times 10^5$ m$^2$. For an assumed spherical flame, the diameter is approximately 295 m. From Section 3.3, the shape factor is

$$F_{T-F} = \frac{295^2}{295^2 + 4R^2} \qquad (4.1)$$

Some nuclear power plants have medium to large natural gas pipelines as close as 500 m from the nearest safety-related structure. For the purposes of this example calculation, standoff distances of 500, 1000, and 1500 m will be used. The incident flux upon the target $P_T$ is given by:

$$Q_i = P_{SU}{}^{TF}{}_{T-F} \qquad (4.2)$$

Using a value of 350 kW/m$^2$ for $P_{SU}$ from Section 3.3, the values for $Q_i$ for the three ranges are:

| Range | $F_{T-F}$ | $Q_i$ |
|---|---|---|
| 500 m | .080 | 19.6 kW/m$^2$ |
| 1000 | .021 | 4.6 |
| 1500 | .010 | 2.0 |

Thus, at slightly under two fire diameters away (500 m), the heat flux on the target is reduced from the specific emission power by a factor of about 18.

The wall response model described in Chapter 2 (Table 2-1) indicates a maximum allowable exposure time of about 9.5 hours for an incident heat flux rate of 20 $kW/m^2$. This is greatly in excess of expected fire durations, as transmissions pipelines have automatic isolation values at regular intervals.

The combination of heat fluxes and exposure durations estimated above are high compared to the heat required to produce third-degree burns on exposed skin. Hardee and Lee[15] give a condition for third-degree burns of 130 $kJ/m^2$ for a 10 to 30 second exposure. This corresponds to heat fluxes of 4 to 13 $kW/m^2$. The short exposure times, as compared to postulated fire durations, could severely restrict personnel movement and emergency response near such a fire.

## 4.2 Gasoline Storage Tank

A typically large storage tank for gasoline and other liquid petrochemicals is on the order of 2-1/2 million gallons (60,000 bbls or 9460 $m^3$). Tank dimensions are 30 m diameter by 14 m high (100' x 40'). For a discharge hole of 1 $m^2$ area, the initial mass flow rate $M_F$ is:

$$M_F = (800\ kg/m^3)(1\ m^2(0.6)[((2) \times (9.8\ m/s^2)(14\ m)]$$

$$= 7950\ kg/s$$

The radiated power $P_R$ is

$$P_R = M_F[\eta\Delta H_C - (T_f - T_a)(\eta S(1 + \chi)C_{pa} + C_{pf})]/10^3$$

where

$\eta$ = fraction of fuel burned

= 1.

$\Delta H_C$ = heat of combustion of fuel

= 1.3 $10^6$ cal/mole[13]

= 4.8 $10^7$ J/kg

$T_f$ = flame temperature or temperature of combustion products

= 1500 K

$T_a$ = initial air temperature

= 300 K

X = fraction of excess air

= 0.25

S = stoichiometric air/fuel ratio

= 15[13]

$C_{pa}$ = mean heat capacity of air

= 1150 J/kg K[13]

$C_{pf}$ = mean heat capacity of fuel

= 1670 J/kg K[13]

Substituting, we have

$$P_R = (7950 \text{ kg/s})\{(1)(4.8 \times 10^7 \text{ J/kg}) - (1500 - 300)[(1)(15)(1.25)(1150 \text{ J/kg K}) + (1670 \text{ J/kg K})]\}$$

$$= (7950 \text{ kg/s})\{4.8 \times 10^7 \text{ J/kg} - 2.8 \times 10^7 \text{ J/kg}\}/10^3$$

$$= 1.6 \times 10^8 \text{ kW}$$

Using a surface emittance of 75 kW/m$^2$ from Section 3.2, the estimated flame surface area is 2.1 x 10$^6$ m$^2$. For an assumed spherical flame shape, the diameter is approximately 820 m. From Section 3.3, the shape factor is

$$F_{T-F} = \frac{820^2}{820^2 + 4R^2} \qquad (4.3)$$

For the three standoff distances used in the previous section, and using a specific emissive power of 150 kW/m$^2$ from Section 3.3, the shape factors, incident radiant energy, and maximum exposure times are

| Range | $F_{T-F}$ | $Q_i$ | $t_{MAX}$ |
|---|---|---|---|
| 500 m | 0.40 | 42 kW/m$^2$ | ~ 5.5 |
| 1000 | 0.14 | 14 | ~12 |
| 1500 | 0.07 | 6.3 | - |

Even at the shortest range, the maximum allowable exposure time is about 5.5 hours. These maximum allowable exposure times should be compared to total fuel consumption times of less than 1 hour (9460 $m^3$ x 800 $kg/m^3$ ÷ 7950 kg/s).

## 4.3 NG Pipeline (1/2') and Comparison With Tests

As part of a series of tests involving extinguishment of natural gas fires, measurements were made of the flame size and fuel flow rate.[16] Their correlation for flame area versus fuel flow rate V (in standard cubic feet per second) is

$$A \sim 122\ V^{2/3} \qquad (4.4)$$

Their largest fuel flow rate was approximately 2600 $ft^3/sec$, which gives a flame surface area of 23100 $ft^2$ (2150 $m^2$).

Applying the methodology of this report, the fuel flow rate is 52.6 kg/s and the radiated thermal power is $1.26 \times 10^9$ W. Using a value of 150 $kW/m^2$ for the specific emissive power gives a flame surface area of 8400 $m^2$. This is a factor of 4 larger than the experimental data, suggesting that a more realistic or central estimate for the surface emittance might be more appropriate for calculating the flame surface area. Using 300 $kW/m^2$ gives an area of 4200 $m^2$. Other parameters which could affect these estimates include combustion efficiency, fraction of excess entrained air, and flame temperature.

# 5.0 SUMMARY

The vulnerability of and hazards to nuclear power plant structures arising from large, external fires is examined. The inherent vulnerability of a plant is the capacity of the concrete safety-related structures to absorb thermal loads without exceeding the thermal and structural design criteria.

First, the passive capacity of reinforced concrete panels to absorb high heat fluxes was determined. The range of heat fluxes considered was 15 to 1400 $kW/m^2$. The latter corresponds to the emissive power of a gas volume radiating as a black body at the adiabatic flame temperature. Two phenomena were considered: heat conduction into the wall, and, for heat fluxes above 350 $kW/m^2$, ablation or erosion of the front surface. Reradiation heat loss effects at the exposed concrete surface are included. For each value of the heat flux, three criteria were used to determine the maximum allowable exposure time:

1. Maximum temperature at the first rebar location of 177°C (350°F); short-term bulk ACI and ASME criteria.

2. For high heat fluxes, erosion limited to 1/2 the distance to the first rebar.

3. Maximum temperature at the inside surface of the wall of 50°C (120°F).

For heat fluxes above 500 $kW/m^2$, the erosion criterion applies. Below this flux, the first criterion defines the acceptable exposure duration of the fire. For the range of heat fluxes considered (15 to 1400 $kW/m^2$), the temperature limit of the third criterion is never reached. Therefore, it may be concluded that external fire events pose no direct threat to safety-related equipment or systems located inside concrete power plant structures.

Second, a relatively simple model for estimating the thermal output of large fires was developed. Based on the estimated fuel flow rate and the total thermal energy produced, the experimentally observed specific power emitted from the surface of large flames was used to estimate the emitting area and the flame size. Using an assumed spherical flame shape, the view factor and the heat flux incident upon the target are developed as a function of range.

To help in accident evaluations, methods are presented for estimating fuel flow rates for high-pressure natural gas pipelines and large liquid petrochemical storage tanks.

Three example calculations are presented: rupture of a 0.91 m (3') NG pipeline, a 1 $m^2$ hole in a 2.5 M gallon gasoline tank, and rupture of a 0.15 m (1/2') NG pipeline (including comparison with experimental data). For a fire to plant range of only 500 m, none of these accidents would pose a threat to the safety-related structures of a nuclear power plant based on the combinations of heat flux and exposure duration given in Table 2-1 and Figure 2-6.

One of the original goals of this study was to develop for general use an explicit (graphical) relationship between the maximum allowable exposure time and the range, for several selected values of the fuel flow rate. The results of Chapters 3 and 4 show that only very large fires at close ranges produce heat fluxes on the target above the lowest value considered, 15 $kW/m^2$, which corresponds to an exposure time of 12 hours. While the graphical relationship could not be developed in a useful form for standoff distances of interest (>500 m); the analysis methods can still be applied on a case-by-case basis.

## REFERENCES


1. Bennett, D. E., and N. C. Finley, "Hazards to Nuclear Power Plants From Nearby Accidents Involving Hazardous Materials--A Preliminary Assessment," Sandia National Laboratories, Albuquerque, New Mexico, SAND80-2334, NUREG/CR-1748, April 1981.

2. American Concrete Institute, Sections SP-4, SP-55.

3. American Society of Mechanical Engineers, Code Section III. 440.

4. Parker, R. O., "Calculating Thermal Radiation Hazards in Large Fires," Fire Technology, Vol. 10, May 1974, pp. 147-152.

5. Harmathy, T. Z., and L. W. Allen, "Thermal Properties of Selected Masonry Unit Concrete," American Concrete Institute Journal, February 1973, pp. 132-142.

6. Muir, J. F., "Response of Concrete Exposed to a High Heat Flux on One Surface," November 1977, SAND77-1467, Sandia National Laboratories, Albuquerque, New Mexico.

7. Chu, T. Y., "Radiant Heat Evaluation of Concrete--A Study of the Erosion of Concrete Due to Surface Heating," January 1978, SAND77-0922, Sandia Laboratories, Albuquerque, New Mexico.

8. Lewis, D. R., J. D. Gaski, and L. R. Thompson, "CINDA-3G-Chrysler Improved Numerical Differencing Analyzer for Third Generation Computers," Report NASA-CR-99595, National Aeronautics and Space Administration, October 20, 1967.

9. Siegel, R., and J. R. Howell, Thermal Radiation Heat Transfer, McGraw-Hill Book Co., New York, NY, Second Edition, 1981.

10. Hottel, H. C., and A. F. Sarofim, Radiative Transfer, McGraw-Hill Book Co., New York, NY, 1967.

11. Raj, P. K., "Atmospheric Attenuation of Thermal Radiation, Exhibit 1005, Rebuttal Testimony," Docket CP-73-47, CP-73-132, et al, Hearings before FPC, February 1976.

12. Cline, D. D., and L. N. Koenig, "The Transient Growth of an Unconfined Pool Fire," Sandia National Laboratories, Albuquerque, New Mexico, SAND82-1512J, to appear in Fire Technology, May 1983.

13. Bolz, R. E., and G. L. Tuve, Editors, Handbook of Tables for Applied Engineering Science, Second Edition, The Chemical Rubber Co., Cleveland, Ohio, 1976.

14. Raj, P. K., N. A. Moussa, K. Aravamudan, and C. D. Lind, "LNG Spill Fire Tests on Water--An Overview of the Results," Proceedings Transmission Conference, American Gas Association, May 21-23, 1979, New Orleans, Louisiana, #79-T-50.

15. Hardee, H. C., and D. O. Lee, "A Simple Conduction Model for Skin Burns Resulting From Exposure to Chemical Fireballs," Fire Research, 1, 199-205, (1977/78).

16. Guise, A. B., "Extinguishment of Natural Gas Pressure Fires," Fire Technology, Vol. 3, pp. 175-193, 1967.

17. Structural Analysis and Design of Nuclear Plant Facilities, Committee on Nuclear Structures and Materials, Structural Division, American Society of Civil Engineers, New York, NY. Manuals and Reports on Engineering Practice, No. 58, 1980.

18. Natural Gas Survey, Volume III, Transmission, Task Force Reports, Federal Power Commission, Washington, DC, 1973, p. 128.

19. Hardee, H. C., D. O. Lee, and W. B. Benedick, "Thermal Hazards From LNG Fireballs," Combustion Science and Technology, Vol. 17, pp. 189-197, 1978.

20. Steward, F. R., "Linear Flame Heights for Various Fuels," Combustion and Flame, Vol. 18, pp. 171-178, 1964.

21. Steward, F. R., "Prediction of the Height of Turbulent Diffusion Bouyant Flames," Combustion Science and Technology, Vol. 2, pp. 203-212, 1970.

22. Zukoski, E. E., T. Kubota, and B. Cetegen, "Entrainment in Fire Plumes," National Bureau of Standards, Washington, DC, NBS-GCR-80-294, March 1981.

## 6.0 APPENDIX--DISCHARGE FROM A HIGH-PRESSURE NATURAL GAS PIPELINE

The rupture and subsequent discharge of a high-pressure natural gas pipeline is a time-dependent blowdown problem. The exit mass flow rate is a complex decaying function of time, in addition to being dependent on accident conditions (eg, hole shape, roughness, orientation, etc). A simpler approach is to evaluate steady-state flow rates which will bound the problem. For the purposes of safety analyses, such an approach is both sufficient and conservative.

Let us consider a pipeline of diameter D, cross-sectional area A, initial pressure P, and initial temperature T filled with natural gas. For typical US pipelines, the initial conditions are:

$$T = 300 \text{ K}$$
$$P = 6.9 \cdot 10^6 \text{ Pa (1000 psi)}$$
$$\rho = 44.4 \text{ kg/m}$$

where $\rho$ is the density. The normal transmission velocity of 10 to 15 m/s (25 to 35 mph) can be neglected in the blowdown analysis. Sizes range up to 1.07 m (3-1/2') in diameter; this analysis will consider 6 sizes from 0.15 m (1/2') to 1.07 m (3-1/2').

The discharge flow rate $M_F$ is given by:

$$M_F = \rho AV = \rho AMC$$

where V is the discharge velocity, M is the Mach number, and C is the sound speed. Immediately after rupture of the pipeline, the flow velocity is near sonic ($M \cong 1$). For an ideal gas, the sound speed is given by

$$C = (\gamma RT)^{1/2}$$

where R is the gas constant (518.2 J/kg K for methane), and $\gamma$ is the ratio of the specific heats. In Table A-1, this maximum discharge flow rate is listed in the fifth column. In the first four columns are the diameter, cross-sectional area, volume of a 30 km length of pipeline and the total mass contained in the 30 km length. The choice of 30 km is based on a reasonable but still conservative estimate of the distance between automatic block (or safety) valves in pipelines.

As the pipeline blows down, the flow can be characterized as adiabatic (or isentropic) with friction between the gas and the pipe wall. The high initial pressure means that the flow is choked; that is, the flow conditions are not

influenced by conditions after the pipe exit (eg, back-pressure or atmospheric pressure). Steady-state, adiabatic flow with friction is described by the Fanno line equations, which are given in several texts.[A1,A2]

A steady state problem consisting of the discharge of a semi-infinite reservoir through a length of pipe, L, is readily solvable. The steady-state flow rates for several pipe lengths should provide reasonable estimates for actual blowdown flow rates. The reservoir is assumed to be at the same temperature and pressure as in the pipeline prior to the accident. For this analysis, two pipe lengths of 2 and 5 km were chosen. The friction factor was taken to be 0.003.

Tabulated values for the Fanno line equations can be used to estimate the flow velocity at the entrance to the length, given that the exit velocity is sonic (M = 1). In Table A-1, column 6 lists the entrance Mach numbers for the two pipe length, and column 7 lists the corresponding mass flow rates.

A rough estimate of the blowdown time can be made using a fraction of the mass flow rate for the 5 km pipe. For this safety analysis, the fraction was taken to be one-fourth. This, in a sense, represents an "average" flow rate over the entire discharge time. Using the total mass in the pipeline, estimates for the blowdown times are listed in column 8, and they range from about 2 hours for small pipes to less than 3/4 of an hour for large ones. As will be seen, these times are relatively short compared to maximum allowable concrete exposure times.

Estimates of the visible height of turbulent diffusion flames can be made using the correlations developed by Becker and Liang.[A3] Using their notation except for H for the flame height and $M_F$ for the mass flow rate, the appropriate correlation is:

$$\psi = 0.18 + 0.022\xi_H$$

where

$$\psi = \left(\frac{D_S \beta}{H\ W_1}\right)^{2/3}$$

$$\xi_H = H\left(\frac{\pi g\ \rho_\infty}{4\ M_F U_S}\right)^{1/3}$$

$D_S$ = effective source diameter

$$= \left( \frac{4\ M_F}{\pi \rho_\infty U_S} \right)^{1/2}$$

$$\beta = \left( \frac{M_\infty T_1}{M_1 T_\infty} \right)^{1/2}$$

$W_1$ = (1 + air/fuel ratio)$^{-1}$

= (1 + 17)$^{-1}$ = 1/18 for methane

$U_S$ = effective gas velocity at source

= 450 m/s

$g$ = graviational constant

= 9.8 m/s$^2$

$\rho_\infty$ = ambient air density

= 1.29 kg/m$^3$

$M_1$ = mean molecular weight of stoichiometric combustion products at the adiabatic combustion temperature

= 26.7 kg/kg mole

$M_\infty$ = mean molecular weight of air

= 28.8 kg/kg mole

$T_1$ = adiabatic combustion of a stoichiometric air/fuel mixture

= 2220 K

$T_\infty$ = ambient temperature

= 300 K

Performing the substitutions, the equation for $\psi$ reduces to:

$$\frac{1.78\ M_F^{1/3}}{H^{2/3}} = 0.18 + 0.00618\ \frac{H}{M_F^{1/3}}$$

For each of the mass flow rates in Table A-1, this equaton was solved numerically for the estimated flame height. These values are listed in column 9.

Finally, the fire model developed in Sections 3.1 and 3.2 and illustrated in Section 4.1 can be used to estimate the equivalent sphere diameter for fires with the mass flow rates as listed in column 6. The total radiated power is listed in column 10, the flame surface area in column 11 and the equivalent sphere diameter in column 12. The flame heights predicted by the correlations of Becker and Liang range from about twice the sphere diameter for smaller pipelines to about 25 percent greater for large pipelines.

Since large flames would be expected to have height-to-diameter ratios in the range of 2 to 5, the use of the equivalent sphere for estimating fire vulnerability is conservative. That is, the radiating area for an inverted cone (using the height in column 9) would be less than the radiating area for a sphere (column 11).

## REFERENCES


A1. Zucrow, J. J., and J. D. Hoffman, Gas Dynamics, John Wiley and Sons, Inc., New York, 1976.

A2. John, J. E. A., Gas Dynamics, Allyn and Bacon, Boston, 1969.

A3. Becker, H. A., and D. Liang, "Visible Length of Vertical Free Turbulent Diffusion Flames," Combustion and Flame, Vol. 32, pp. 115-137, 1978.

TABLE A-1

Data for Large Pipeline Fires

| Diameter (m) | Cross Sectional Area ($m^2$) | Volume of 30 km Length ($m^3$) | Total Mass In 30 km (kg) | Maximum Flow Rate (kg/s) | Mach Number for 5 km & 2 km Pipes | Mass Flow Rates for 5 km & 2 km Pipes (kg/s) | Discharge Time Using 1/4 of 5 km Rate (hrs) | Flame Height (m) | Total Radiated Power (J) | Flame Surface Area ($m^2$) | Equivalent Sphere Diameter (m) |
|---|---|---|---|---|---|---|---|---|---|---|---|
| .15 | .018 | 5.3E2 | 2.4E4 | 3.5E2 | .04 | 14 | 1.9 | 51 | 3.4E8 | 2.2E3 | 27 |
| (.5') | | | | | .07 | 35 | | 66 | 6.0E8 | 4.0E3 | 36 |
| .30 | .071 | 2.1E3 | 9.3E4 | 1.4E3 | .06 | 80 | 1.3 | 110 | 1.9E9 | 1.3E4 | 64 |
| (1') | | | | | .10 | 140 | | 140 | 3.4E9 | 2.2E4 | 84 |
| .45 | .16 | 4.8E3 | 2.1E5 | 3.2E3 | .07 | 220 | 1.1 | 170 | 5.3E9 | 3.5E4 | 110 |
| (1.5') | | | | | .12 | 380 | | 210 | 9.1E9 | 6.1E4 | 140 |
| .61 | .29 | 8.8E3 | 3.9E5 | 5.8E3 | .09 | 520 | .8 | 240 | 1.3E10 | 8.3E4 | 160 |
| (2') | | | | | .14 | 810 | | 290 | 1.9E10 | 1.3E5 | 200 |
| .91 | .64 | 1.9E4 | 8.5E5 | 1.3E4 | .11 | 1400 | .7 | 370 | 3.4E10 | 2.2E5 | 270 |
| (3') | | | | | .16 | 2100 | | 440 | 5.0E10 | 3.4E5 | 330 |
| 1.07 | .90 | 2.7E4 | 1.2E6 | 1.8E4 | .11 | 2000 | .7 | 430 | 4.8E10 | 3.2E5 | 320 |
| (3.5') | | | | | .18 | 3200 | | 530 | 7.7E10 | 5.1E5 | 400 |

Distribution

US NRC Distribution Contractor (CDSI)
7300 Pearl Street
Bethesda, MD 20014
405 Copies for R4, RP

Kenneth G. Murphy (5)
Division of Risk Analysis
US Nuclear Regulatory Commission
Washington, DC 20555

1510 D. B. Hayes
1513 D. W. Larson
1513 D. D. Cline (5)
1520 T. B. Lane
1824 J. N. Sweet
3141 L. J. Erickson (5)
3151 W. L. Garner
6255 D. O. Lee
6400 A. W. Snyder
6410 D. J. McCloskey
6412 J. W. Hickman
Attn: G. J. Kolb
6414 D. M. Ericson, Jr.
6414 D. L. Berry
6415 D. C. Aldrich
6415 D. E. Bennett (20)
6422 D. A. Powers
6440 D. A. Dahlgren
6442 W. A. Von Riesemann
6443 D. D. Carlson
6446 B. E. Bader
6448 L. O. Cropp
7530 W. E. Caldes
8214 M. A. Pound

NRC FORM 335 (11-81) U.S. NUCLEAR REGULATORY COMMISSION

**BIBLIOGRAPHIC DATA SHEET**

1. REPORT NUMBER *(Assigned by DDC)*
NUREG/CR-3330
SAND83-1178

4. TITLE AND SUBTITLE *(Add Volume No., if appropriate)*
VULNERABILITY OF NUCLEAR POWER PLANT STRUCTURES TO LARGE EXTERNAL FIRES

2. *(Leave blank)*

3. RECIPIENT'S ACCESSION NO.

7. AUTHOR(S)
David E. Bennett

5. DATE REPORT COMPLETED
MONTH: August YEAR: 1983

9. PERFORMING ORGANIZATION NAME AND MAILING ADDRESS *(Include Zip Code)*
Sandia National Laboratories
Albuquerque, NM 87185

DATE REPORT ISSUED
MONTH: September YEAR: 1983

6. *(Leave blank)*

8. *(Leave blank)*

12. SPONSORING ORGANIZATION NAME AND MAILING ADDRESS *(Include Zip Code)*
Division of Risk Analysis
Office of Nuclear Regulatory Research
U.S. Nuclear Regulatory Commission
Washington, DC 20555

10. PROJECT/TASK/WORK UNIT NO.

11. FIN NO.
A1214

13. TYPE OF REPORT
Technical

PERIOD COVERED *(Inclusive dates)*

15. SUPPLEMENTARY NOTES

14. *(Leave blank)*

16. ABSTRACT *(200 words or less)*

This report examines the inherent vulnerability of nuclear power plant structures to the thermal environments arising from large, external fires. The inherent vulnerability is the capacity of the concrete safety-related structures to absorb thermal loads without exceeding the appropriate thermal and structural design criteria. The potential sources of these thermal environments are large, offsite fires arising from accidents involving the transportation or storage of large quantities of flammable gases or liquids.

A realistic thermal response analysis of a concrete panel was performed using three limiting criteria: temperature at the first rebar location, erosion and ablation of the front (exterior) surface due to high heat fluxes, and temperature at the back (interior) surface. The results of this analysis yield a relationship between incident heat flux and the maximum allowable exposure duration.

A simple fire analysis method was developed to predict the thermal flux incident upon a target as a function of range. A key feature is the use of an experimentally observed specific power emitted from the surface of large fires.

Example calculations for the break of a 0.91 m (3') diameter high-pressure natural gas pipeline and a 1 $m^2$ hole in a 2-1/2 million gallon gasoline tank show that the resulting fires do not pose a significant hazard for ranges of 500 m or greater.

17. KEY WORDS AND DOCUMENT ANALYSIS

17b. IDENTIFIERS/OPEN-ENDED TERMS

18. AVAILABILITY STATEMENT
Unlimited

19. SECURITY CLASS *(This report)*
Unclassified

21. NO. OF PAGES
37

20. SECURITY CLASS *(This page)*
Unclassified

22. PRICE
$

| Org. | Bldg. | Name | Rec'd by | Org. | Bldg. | Name | Rec'd by |
|---|---|---|---|---|---|---|---|
| | | | | | | | |
| | | | | | | | |
| | | | | | | | |
| | | | | | | | |
| | | | | | | | |
| | | | | | | | |
| | | | | | | | |
| | | | | | | | |
| | | | | | | | |
| | | | | | | | |
| | | | | | | | |
| | | | | | | | |
| | | | | | | | |
| | | | | | | | |
| | | | | | | | |

Sandia National Laboratories